7

Computation of Harmonic Flows

7.1 Introduction

Although the title specifically refers to *harmonic flows*, the analysis and algorithms described in this chapter are equally applicable to other frequencies in the region of interest such as inter-harmonics and subharmonics.

The simplest harmonic flow involves a single harmonic source and single-phase network analysis. This model is commonly used to derive the system harmonic impedances at the point of common coupling in filter design. In general, however, the network will be unbalanced and may contain several harmonic sources. Therefore, the derivation of the harmonic voltages and currents requires multi-source three-phase harmonic analysis. If the harmonics generated by the nonlinear components are reasonably independent of the voltage distortion level in the a.c. system, the derivation of the harmonic sources (the subject of Chapter 3) can be decoupled from the analysis of harmonic penetration and a direct (nodal) solution is possible. Since most nonlinearities manifest themselves as harmonic current sources, this is normally called the current injection method. In such cases, the expected voltage levels or the results of a fundamental frequency load flow are used to derive the current waveforms, and with them the harmonic content of the nonlinear components.

After a description of the direct harmonic analysis algorithm, the following sections discuss the modelling of network components and the formulation of the nodal admittance matrix as well as the computer implementation of the harmonic flow algorithm.

7.2 Direct Harmonic Analysis

The distribution of voltage and current harmonics throughout a linear power network containing one or more harmonic current sources is normally carried out using nodal analysis [1]. The asymmetry inherent in transmission systems cannot be studied with any simplification by using the symmetrical component frame of reference, therefore phase components are used.

Power System Harmonics, Second Edition J. Arrillaga, N.R. Watson
 ISBN: 0-470-85129-5

The nodal admittance matrix of the network at frequency f is of the form

$$[Y_f] = \begin{bmatrix} Y_{11} & Y_{12} & \dots & Y_{1i} & \dots & Y_{1k} & \dots & Y_{1n} \\ Y_{21} & Y_{22} & \dots & Y_{2i} & \dots & Y_{2k} & \dots & Y_{2n} \\ \vdots & \vdots & \ddots & \vdots & \ddots & \vdots & \ddots & \\ Y_{i1} & Y_{i2} & \dots & Y_{ii} & \dots & Y_{ik} & \dots & Y_{in} \\ \vdots & \vdots & \ddots & \vdots & \ddots & \vdots & \ddots & \\ Y_{k1} & Y_{k2} & \dots & Y_{ki} & \dots & Y_{kk} & \dots & Y_{kn} \\ \vdots & \vdots & \ddots & \vdots & \ddots & \vdots & \ddots & \\ Y_{n1} & Y_{n2} & \dots & Y_{ni} & \dots & Y_{nk} & \dots & Y_{nn} \end{bmatrix} \tag{7.1}$$

where Y_{ki} is the mutual admittance between busbars k and i at frequency f, and Y_{ii} is the self-admittance of busbar i at frequency f.

A separate system admittance matrix is generated for each frequency of interest. The main difficulty is to determine which model best represents the various system components at the required frequency and obtain appropriate parameters for them. With this information, it is straightforward to build up the system fundamental and harmonic frequency admittance matrices.

The three-phase nature of the power system always results in some load or transmission line asymmetry, as well as circuit coupling. These effects give rise to unbalanced self- and mutual admittances of the network elements.

For the three-phase system, the elements of the admittance matrix are themselves 3×3 matrices consisting of self- and transfer admittances between phases, i.e.

$$Y_{ii} = \begin{bmatrix} Y_{aa} & Y_{ab} & Y_{ac} \\ Y_{ba} & Y_{bb} & Y_{bc} \\ Y_{ca} & Y_{cb} & Y_{cc} \end{bmatrix} \tag{7.2}$$

Figure 7.1 shows a case of two three-phase harmonic sources and an unbalanced a.c. system. The current injections, i.e. $I_{1h} - I_{3h}$ and $I_{4h} - I_{6h}$, can be unbalanced in magnitude and phase angle.

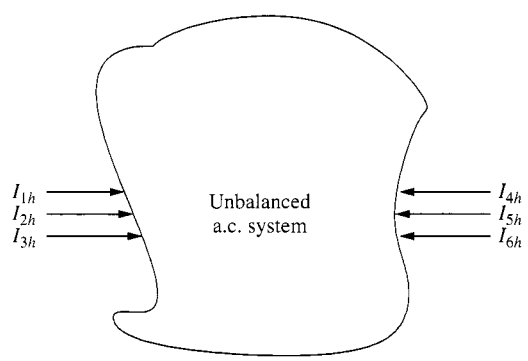

Figure 7.1 Unbalanced current injection into an unbalanced a.c. system

The system harmonic voltages are calculated by direct solution of the linear equation

$$[I_h] = [Y_h]\,[V_h] \qquad \text{for } h \neq 1 \tag{7.3}$$

where $[Y_h]$ is the system admittance matrix.

Therefore, the direct solution involves $h - 1$ independent sets of linear simultaneous equations, i.e.

$$\begin{array}{ccc} [I_h] & = & [Y_h]\ \ [V_h] \\ \cdot & & \cdot\ \ \cdot \\ \cdot & & \cdot\ \ \cdot \\ \cdot[I_3] & = & [Y_3]\ \ \cdot[V_3] \\ [I_2] & = & [Y_2]\ \ [V_2] \end{array} \tag{7.4}$$

The injected currents at most a.c. busbars will be zero, since the sources of the harmonic considered are the nonlinear devices. To calculate an admittance matrix for the reduced portion of a system comprising just the injection busbars, the admittance matrix is formed with those buses at which harmonic injection occurs ordered last. Advantage is taken of the symmetry and sparsity of the admittance matrix [2], by using a row ordering technique to reduce the amount of off-diagonal element build-up. The matrix is triangulated using Gaussian elimination, down to but excluding the rows of the specified buses.

The resulting matrix equation for an n-node system with $n - j + 1$ injection points is

$$\begin{bmatrix} 0 \\ \vdots \\ 0 \\ \hline I_j \\ \vdots \\ I_n \end{bmatrix} = \left[\begin{array}{ccc} & 0 & \\ \hline & Y_{jj} \ \ \ldots \ \ Y_{jn} & \\ 0 & \vdots \qquad\ \ \vdots & \\ & Y_{nj} \ \ \ldots \ \ Y_{nn} & \end{array}\right] \cdot \begin{bmatrix} V_1 \\ \vdots \\ V_{j-1} \\ \hline V_j \\ \vdots \\ V_n \end{bmatrix} \tag{7.5}$$

As a consequence, $I_j \ldots I_n$ remain unchanged since the currents above these in the current vector are zero. The reduced matrix equation is

$$\begin{bmatrix} I_j \\ \vdots \\ I_n \end{bmatrix} = \begin{bmatrix} Y_{jj} & \ldots & Y_{jn} \\ \vdots & \ldots & \vdots \\ Y_{nj} & \ldots & Y_{nn} \end{bmatrix} \cdot \begin{bmatrix} V_j \\ \vdots \\ V_n \end{bmatrix} \tag{7.6}$$

and the order of the admittance matrix is three times the number of injection busbars for a three-phase system. The elements are the self- and transfer admittances of the reduced system as viewed from the injection busbars. Whenever required, the impedance matrix may be obtained for the reduced system by matrix inversion.

Reducing a system to provide an equivalent admittance matrix, as viewed from a specific bus, is an essential part of filter design. The reduction of the admittance matrix to a set of busbars where nonlinearities exist is an essential step to allow accurate

a.c. system representation in many other types of analysis, such as iterative harmonic analysis or as frequency-dependent equivalents in time-domain analysis.

7.2.1 Frequency Scan Analysis

The simplest application of the direct method described above is the frequency scan. It involves the derivation of the frequency response of a network looking from a specified busbar. A one per unit sinusoidal current is injected into the bus at a range of frequencies and the set of equations (7.3) is used to calculate the voltage response. This calculation is repeated at discrete frequency steps covering the specified frequency spectrum.

This process can be equally used with phase or sequence components. In the latter case, one per unit positive- or zero-sequence current is injected to derive the positive- or zero-sequence driving-point network impedances seen from the specified bus.

Frequency scan analysis is widely used in filter design. It is also a preliminary step in the derivation of frequency-dependent equivalents for use in electromagnetic transients simulation.

Instead of injecting one per unit current, the use of one per unit voltage can be used to investigate the effect of background harmonic voltages present at any specified point in the network. The set of equations (7.3) is then used to derive the harmonic voltage transfer to the rest of the network.

7.2.2 Incorporation of Harmonic Voltage Sources

Most power system nonlinearities manifest themselves as harmonic current sources, but sometimes harmonic voltage sources are used to represent the distortion background present in the network prior to the installation of the new nonlinear load. Moreover, some recent power electronic devices based on GTO and IGBT switching, act as voltage sources behind an impedance.

A system containing harmonic voltages at some busbars and harmonic current injections at other busbars is solved by partitioning the admittance matrix and performing a partial inversion. This then allows the unknown busbar voltages and unknown harmonic currents to be found. If V_2 represents the known voltage sources then I_2 are the unknown variables. The remaining busbars are represented as a harmonic current injection I_1 (which can be either zero or specified by harmonic current source) and the corresponding harmonic voltage vector V_1 represents the unknown variables.

Partitioning the matrix equation to separate the two types of nodes gives

$$\begin{bmatrix} Y_{11} & Y_{12} \\ Y_{21} & Y_{22} \end{bmatrix} \begin{bmatrix} V_1 \\ V_2 \end{bmatrix} = \begin{bmatrix} I_1 \\ I_2 \end{bmatrix} \tag{7.7}$$

The unknown voltage vector V_1 is found by solving

$$[Y_{11}]\,[V_1] = [I_1] - [Y_{12}]\,[V_2] \tag{7.8}$$

The harmonic currents injected by the harmonic voltage sources are then found by solving

$$[Y_{21}]\,[V_1] + [Y_{22}]\,[V_2] = [I_2] \tag{7.9}$$

With this formulation some extra processing is required to obtain the reduced admittance matrix, which is not generated as part of the solution.

7.2.3 Cascading Sections

Mutually coupled transmission lines with different tower geometries over the line length need special consideration. If only terminal voltage information is required, the line sections may be combined into one equivalent section using *ABCD* parameters, as shown in Figure 7.2.

All the individual sections must contain the same number of mutually coupled three-phase elements, to ensure that the parameter matrices are of the same order and that matrix multiplications are executable. In this respect, uncoupled sections will use the coupled format with zero coupling elements to maintain the correct dimensions.

For the case of a non-homogeneous line with n different sections

$$\begin{bmatrix} V_S \\ I_S \end{bmatrix} = \begin{bmatrix} [A_1]\,[B_1] \\ [C_1]\,[D_1] \end{bmatrix} \times \begin{bmatrix} [A_2]\,[B_2] \\ [C_2]\,[D_2] \end{bmatrix} \times \cdots \times \begin{bmatrix} [A_n]\,[B_n] \\ [C_n]\,[D_n] \end{bmatrix} \begin{bmatrix} V_R \\ -I_R \end{bmatrix}$$

$$\begin{bmatrix} V_S \\ I_S \end{bmatrix} = \begin{bmatrix} [A]\,[B] \\ [C]\,[D] \end{bmatrix} \begin{bmatrix} V_R \\ -I_R \end{bmatrix} \tag{7.10}$$

It must be noted that in general $[A] \neq [D]$ for a non-homogeneous line.

Once the resultant *ABCD* parameters have been found, the equivalent nodal admittance matrix for the subsystem can be calculated from

$$[Y] = \begin{bmatrix} [D]\,[B]^{-1} & [C] - [D]\,[B]^{-1}[A] \\ [B]^{-1} & -[B]^{-1}[A] \end{bmatrix}. \tag{7.11}$$

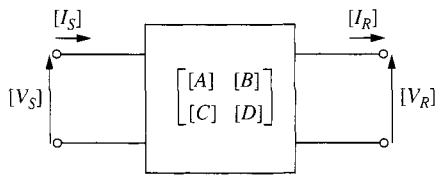

(a)

$$\begin{bmatrix} V_S \\ I_S \end{bmatrix} = \begin{bmatrix} [A] & [B] \\ [C] & [D] \end{bmatrix} \begin{bmatrix} V_R \\ -I_R \end{bmatrix}$$

(b)

Figure 7.2 Two-port network transmission parameters: (a) multi-two-port network; (b) matrix transmission parameters

If, however, extra information along the line is required, appropriate fictitious nodes are created at specified points and/or at regular intervals, and the following nodal matrix equation is formed, inverted (factorised) and solved. The resultant vector provides the harmonic voltage profile along the line. Alternatively, instead of creating fictitious nodes during the solution, and thus increasing the computation, a more detailed voltage profile can be derived by analysing the harmonic flow along the line once the overall solution has been obtained.

$$\begin{bmatrix} I_S \\ I_1 \\ I_2 \\ \vdots \\ I_n \\ I_R \end{bmatrix}_h = \begin{bmatrix} [Y_{SS}] & -[Y_{S1}] & & & & \\ -[Y_{1S}] & [Y_{SS}]+[Y_{11}] & -[Y_{12}] & & & \\ & -[Y_{21}] & [Y_{11}]+[Y_{22}] & \ddots & & \\ & & \ddots & \ddots & \ddots & \\ & & & \ddots & [Y_{nn}]+[Y_{RR}] & -[Y_{nR}] \\ & & & & -[Y_{Rn}] & [Y_{RR}] \end{bmatrix}_h \begin{bmatrix} V_S \\ V_1 \\ V_2 \\ \vdots \\ V_n \\ V_R \end{bmatrix}_h \tag{7.12}$$

7.3 Derivation of Network Harmonic Impedances from Field Tests

In the absence of more accurate information, existing harmonic standards and recommendations often refer to harmonic impedance sources derived from the balanced short-circuit impedance of the system at fundamental frequency. The inadequacy of such an approach has become apparent with the help of online tests and computer studies.

The availability of voltage and current transducers throughout the power system provides the basis for the indirect derivation of harmonic impedances. Their assessment is therefore dependent on the performance of such transducers, which may not have been designed to respond accurately to harmonic frequencies.

The present techniques for the derivation of harmonic impedances can be divided into three groups, depending on the origin of harmonics or inter-harmonics:

- Use of existing harmonics sources (non-invasive)
- Direct injection (invasive)
- Analysis of transient waveforms (non-invasive).

7.3.1 Use of Existing Sources (Online Non-Invasive Tests)

In the non-invasive test the information required is obtained purely from measurements of existing waveforms, i.e. using the harmonic content already present in the system. This is the simplest and most commonly used technique.

Electricit de France [3] has proposed two alternative ways of deriving information on harmonic impedances, in the form of sequence components, using the principle of digital filtering rather than Fourier analysis. One method uses numerical techniques to perform the digital filtering of the physical input values, and retains only the frequencies contained in a selected bandwidth. The information is then used to identify the network with a simple impedance model which is only valid over a relatively narrow frequency range. The identification is carried out separately for the zero-sequence and positive-(negative-) sequence values. The second method uses electronic filters to transform the six voltage and current values into four (two zero-sequence and two positive-sequence), after eliminating the 50 Hz component.

The harmonic content produced by an existing high-voltage d.c. converter station has been used [4] to obtain the harmonic impedances directly from the ratios of voltage and current readings. This assumes that all other important harmonic sources in the power system are disconnected; however, measurements taken without the existing high-voltage d.c. converter station operating, or operating at a different operating point, could have been used to account for the other harmonic sources in the system.

When the harmonic voltage levels are high and affected by the connection of a shunt capacitor bank the method illustrated in Figure 7.3 has been used to identify the main source of harmonics.

The harmonic current injection and harmonic impedances (for the Norton equivalents) are obtained by solving the linear set of equations

$$\begin{bmatrix} 1 & 0 & -V'_m & 0 \\ 0 & -1 & 0 & V'_m \\ 1 & 0 & -V''_m & 0 \\ 0 & -1 & 0 & V''_m \end{bmatrix} \begin{bmatrix} I_1 \\ I_2 \\ Y_1 \\ Y_2 \end{bmatrix} = \begin{bmatrix} I'_m \\ I'_m \\ I''_m \\ I''_m - Y_c V''_m \end{bmatrix} \tag{7.13}$$

where V'_m and I'_m are the measured harmonic voltage and current prior to connecting the capacitor and V''_m and I''_m after.

This method assumes that the components of the Norton equivalents are not affected by the switching operation. In general, however, this is not the case as the related variation in the system harmonic impedances, and particularly their phase angle variation [5], can have considerable effect on the Norton equivalent impedances of the nonlinear load.

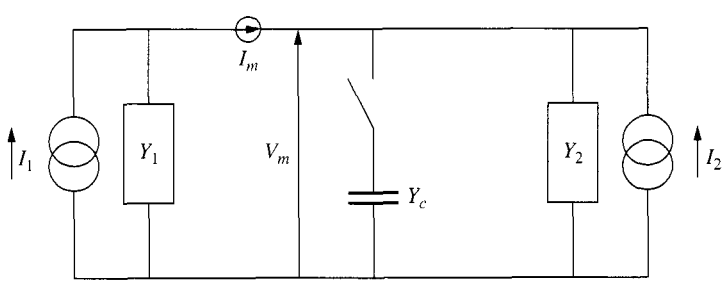

Figure 7.3 Identification of main harmonic source by capacitor switching

7.3.2 Direct Injection (Online Invasive Tests)

In principle, it is possible to design a source of harmonic power which absorbs fundamental frequency power and converts it into harmonic power of the appropriate frequencies, magnitudes and phases. However, the measurement of harmonic impedance requires a distorting source of considerable capacity.

In practice, measurements are usually taken at points where there is considerable distortion due to existing harmonic sources in the network. The effect of injecting a further source needed for harmonic measurement is superimposed on these. The result is a low signal to noise ratio, which makes the measurement unreliable.

To overcome this problem, the Electricity Council Centre (Capenhurst, UK) [6] designed a system which generates power at frequencies mid-way between the characteristic harmonic frequencies of interest, i.e. at the odd multiples of 25 Hz, on the assumption that interpolation between these frequencies is justifiable. The power ratings of the distorting source for measurements at 11 kV, 33 kV and 132 kV are 9 kW, 36 kW and 180 kW, respectively, and the units consist of a switching modulator in series with a resistive load in the form of a fan heater. The 11 kV and 33 kV systems are portable and the 132 kV system is located in a purpose-built van.

Figure 7.4 illustrates the results of typical measurements carried out with this equipment in combination with a harmonic impedance instrument [7], specially designed to provide simultaneous information about voltage and current with their phase relationship.

7.3.3 From Transient Waveforms (Online Non-Invasive Tests)

The methods discussed above involve measurement of the steady-state levels of particular frequencies. Alternatively, the network frequency characteristics can be derived

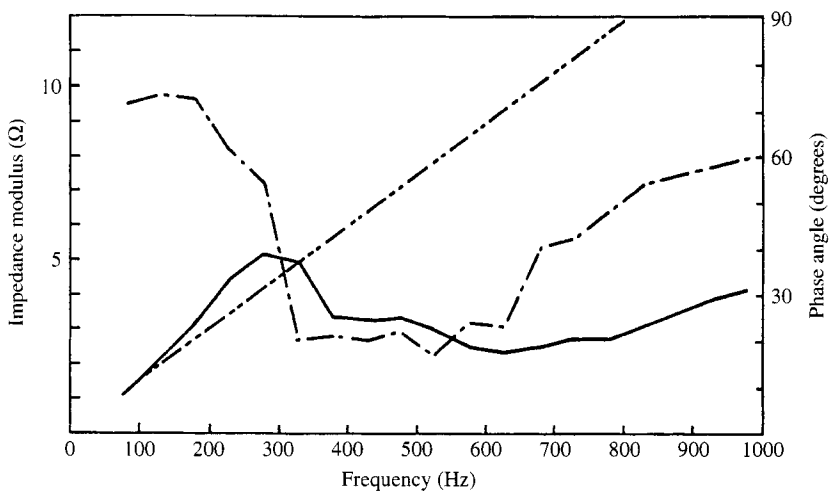

Figure 7.4 Source impedance seen from an 11 kV busbar supplying a commercial load: (· · –· · –), Obtained from the short-circuit impedance at 50 Hz; (———), measured impedance magnitude; (– · – ·), measured impedance phase angle

from the transient voltage and current waveforms produced by normal switching operations. These include the switching of capacitor banks and transformers or even the system natural variations [8].

The advantage of using capacitor banks is their widespread use and their frequent switching, which produces a rich spectrum of inter-harmonics. However, the resulting harmonic currents are unsymmetrical, of short duration and depend on the point of wave of switching.

The transient inrush current produced by transformer switching produces high harmonic current levels compared to existing harmonics with a spectrum, ranging from 100 Hz to about 7000 Hz. Moreover, the signals are present for several seconds. Again the currents are highly unsymmetrical and depend on the switching moment and core remanence.

The use of natural system variations for spectral analysis can also provide time-dependent system impedances. Although this method is generally applicable, it can only achieve good precision in the presence of some predominant disturbing load.

The accuracy of applying the FFT to the voltage and current time-domain recordings in the presence of noise can be improved by correlation analysis in conjunction with spectral analysis. Spectral analysis of the auto- and cross-power spectra has been used to determine the frequency response of two 26.6 kV feeders [9] and also to determine the 3×3 impedance matrices [10]. With these methods, correlation indices are used to reject measurements where the signal to noise ratio causes the calculated values to be suspect. With least squares estimates, the matrix condition number also indicates the accuracy of the answer.

Identification techniques that do not require the use of FFT have also been applied to time-domain responses. Prony analysis and the direct ARMA method are two identification techniques suitable for determining frequency characteristics [11] from time-domain waveforms.

The main advantage of these non-invasive techniques is that they can be readily applied without the need for special injection equipment; however, they are equally applicable to invasive testing, where an impulse or other frequency-rich signal is injected.

7.4 Transmission Line Models

A transmission line consists of distributed inductance and capacitance, which affect the magnetic and electrostatic conditions of the line, and resistance and conductance, which affect the losses. These electrical parameters are calculated from the line geometry and conductor data. The effects of ground currents and earth wires are included in the calculation of these parameters. The calculated parameters are expressed as a series impedance and shunt admittance per unit length. A simple representation of the line includes the line total inductance, capacitance, resistance and conductance as lumped parameters, as shown in Figure 7.5 (nominal PI model). However, when the line length becomes an appreciable part of the wavelength of the frequency of interest, errors become apparent. Subdividing the line and using cascaded nominal PI sections to represent the line can alleviate this problem. The more nominal PI sections used, the closer the model represents the distributed nature of the line, and hence the more

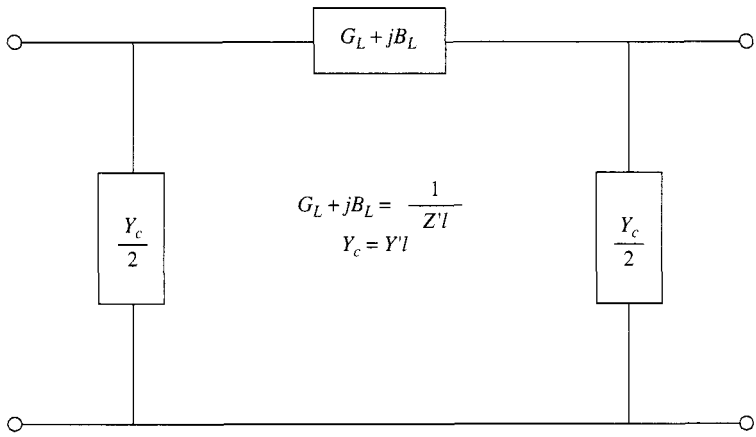

Figure 7.5 Nominal PI representation of transmission line

accurate the model. However, computational burden also greatly increases due to the increase in the number of busbars and lumped elements.

Before considering long line effects in detail, the lumped component representation of a three-phase transmission line with ground wire and earth return, suitable for inclusion in the system admittance matrix, will be considered next.

The impedance of a three-phase transmission line with an overhead earth wire is illustrated in Figure 7.6. Each conductor has resistance, inductance and capacitance, and is mutually coupled to the others.

With respect to Figure 7.6, the following equation can be written for the series impedance equivalent of phase a

$$V_a - V'_a = I_a(R_a + j\omega L_a) + I_b(j\omega L_{ab}) + I_c(j\omega L_{ac}) + j\omega L_{ag} I_g - j\omega L_{an} I_n + V_n \tag{7.14}$$

where

$$V_n = I_n(R_n + j\omega L_n) - I_a j\omega L_{na} - I_b j\omega L_{nb} - I_c j\omega L_{nc} - I_g j\omega L_{ng} \tag{7.15}$$

and substituting

$$I_n = I_a + I_b + I_c + I_g \tag{7.16}$$

gives

$$V_a - V'_a = I_a(R_a + j\omega L_a) + I_b j\omega L_{ab} + I_c j\omega L_{ac} + j\omega L_{ag}\, I_g - j\omega L_{an}\,(I_a + I_b + I_c + I_g) + V_n \tag{7.17}$$

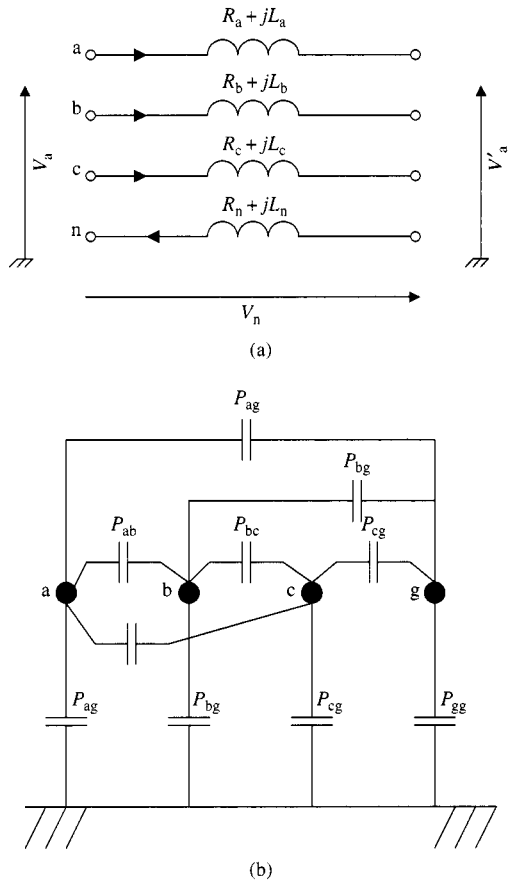

Figure 7.6 (a) Three-phase transmission series impedance equivalent; (b) three-phase transmission shunt impedance equivalent

Regrouping and substituting for V_n, i.e.

$$\begin{aligned}\Delta V_a &= V_a - V'_a \\ &= I_a(R_a + j\omega L_a - j\omega L_{an} + R_n + j\omega L_n - j\omega L_{na}) \\ &\quad + I_b(j\omega L_{ab} - j\omega L_{an} + R_n + j\omega L_n - j\omega L_{nb}) \\ &\quad + I_c(j\omega L_{ac} - j\omega L_{an} + R_n + j\omega L_n - j\omega L_{nc}) \\ &\quad + I_g(j\omega L_{ag} - j\omega L_{an} + R_n + j\omega L_n - j\omega L_{ng}) \qquad (7.18)\end{aligned}$$

$$\begin{aligned}\Delta V_a &= I_a(R_a + j\omega L_a - 2j\omega L_{an} + R_n + j\omega L_n) \\ &\quad + I_b(j\omega L_{ab} - j\omega L_{bn} - j\omega L_{an} + R_n + j\omega L_n) \\ &\quad + I_c(j\omega L_{ac} - j\omega L_{cn} - j\omega L_{an} + R_n + j\omega L_n) \\ &\quad + I_g(j\omega L_{ag} - j\omega L_{gn} - j\omega L_{an} + R_n + j\omega L_n) \qquad (7.19)\end{aligned}$$

or

$$\Delta V_a = Z_{aa-n} I_a + Z_{ab-n} I_b + Z_{ac-n} I_c + Z_{ag-n} I_g \tag{7.20}$$

and writing similar equations for the other phases and earth wire, the following matrix equation results:

$$\begin{bmatrix} \Delta V_a \\ \Delta V_b \\ \Delta V_c \\ \Delta V_g \end{bmatrix} = \begin{bmatrix} Z_{aa-n} & Z_{ab-n} & Z_{ac-n} & Z_{ag-n} \\ Z_{ba-n} & Z_{bb-n} & Z_{bc-n} & Z_{bg-n} \\ Z_{ca-n} & Z_{cb-n} & Z_{cc-n} & Z_{cg-n} \\ Z_{ga-n} & Z_{gb-n} & Z_{gc-n} & Z_{gg-n} \end{bmatrix} \begin{bmatrix} I_a \\ I_b \\ I_c \\ I_g \end{bmatrix} \tag{7.21}$$

Usually we are interested only in the performance of the phase conductors, and it is more convenient to use a three-conductor equivalent for the transmission line. This is achieved by writing matrix equation (7.21) in partitioned form as follows:

$$\begin{bmatrix} \Delta V_{abc} \\ \Delta V_g \end{bmatrix} \quad \begin{bmatrix} Z_A & Z_B \\ Z_C & Z_D \end{bmatrix} \quad \begin{bmatrix} I_{abc} \\ I_g \end{bmatrix} \tag{7.22}$$

From (7.22)

$$[\Delta V_{abc}] = [Z_A]\,[I_{abc}] + [Z_B]\,[I_g] \tag{7.23}$$

$$[\Delta V_g] = [Z_C]\,[I_{abc}] + [Z_D]\,[I_g] \tag{7.24}$$

From equations (7.23) and (7.24), and assuming that the earth wire is at zero potential,

$$[\Delta V_{abc}] = [Z_{abc}]\,[I_{abc}] \tag{7.25}$$

where

$$[Z_{abc}] = [Z_A] - [Z_B]\,[Z_D]^{-1}[Z_C] = \begin{bmatrix} Z'_{aa-n} & Z'_{ab-n} & Z'_{ac-n} \\ Z'_{ba-n} & Z'_{bb-n} & Z'_{bc-n} \\ Z'_{ca-n} & Z'_{cb-n} & Z'_{cc-n} \end{bmatrix} \tag{7.26}$$

With reference to Figure 7.6(b), the potentials of the line conductors are related to the conductor charges by the matrix equation [12]

$$\begin{bmatrix} V_a \\ V_b \\ V_c \\ V_g \end{bmatrix} = \begin{bmatrix} P_{aa} & P_{ab} & P_{ac} & P_{ag} \\ P_{ba} & P_{bb} & P_{bc} & P_{bg} \\ P_{ca} & P_{cb} & P_{cc} & P_{cg} \\ P_{ga} & P_{gb} & P_{gc} & P_{gg} \end{bmatrix} \begin{bmatrix} Q_a \\ Q_b \\ Q_c \\ Q_g \end{bmatrix} \tag{7.27}$$

considerations as for the series impedance matrix, lead to

$$[V_{abc}] = [P'_{abc}]\,[Q_{abc}] \tag{7.28}$$

where P'_{abc} is a 3×3 matrix which includes the effects of the earth wire. The capacitance matrix of the transmission line of Figure 7.6 is given by

$$[C'_{abc}] = [P'_{abc}]^{-1} = \begin{array}{|c|c|c|} \hline C_{aa} & -C_{ab} & -C_{ac} \\ \hline -C_{ba} & C_{bb} & -C_{bc} \\ \hline -C_{ca} & -C_{cb} & C_{cc} \\ \hline \end{array} \tag{7.29}$$

The series impedance and shunt admittance lumped PI model representation of the three-phase line is shown in Figure 7.7(a) and its matrix equivalent is illustrated in Figure 7.7(b). These two matrices can also be represented by compound admittances [13] (Figure 7.7(c)).

Using the compound component concept, the nodal injected currents of Figure 7.7(c) are related to the nodal voltages by the equation

$$\begin{array}{|c|} \hline [I_i] \\ \hline [I_k] \\ \hline \end{array} = \begin{array}{|c|c|} \hline [Z]^{-1} + [Y]/2 & -[Z]^{-1} \\ \hline -[Z]^{-1} & [Z]^{-1} + [Y]/2 \\ \hline \end{array} \begin{array}{|c|} \hline [V_i] \\ \hline [V_k] \\ \hline \end{array} \tag{7.30}$$

$6 \times 1 \qquad 6 \times 6 \qquad 6 \times 1$

This forms the element admittance matrix representation for the short line between busbars i and k in terms of 3×3 matrix quantities.

7.4.1 Mutually Coupled Three-Phase Lines

When two or more transmission lines occupy the same right of way for a considerable length, the electrostatic and electromagnetic coupling between those lines must be taken into account.

Consider the simplest case of two mutually coupled single-circuit three-phase lines. The two coupled lines are considered to form one subsystem composed of four system busbars. The coupled lines are illustrated in Figure 7.8, where each element is a 3×3 compound admittance and all voltages and currents are 3×1 vectors.

The coupled series elements represent the electromagnetic coupling while the coupled shunt elements represent the capacitive or electrostatic coupling. These coupling parameters are lumped in a similar way to the standard line parameters.

With the admittances labelled as in Figure 7.8, and applying the rules of linear transformation for compound networks, the admittance matrix for the subsystem is

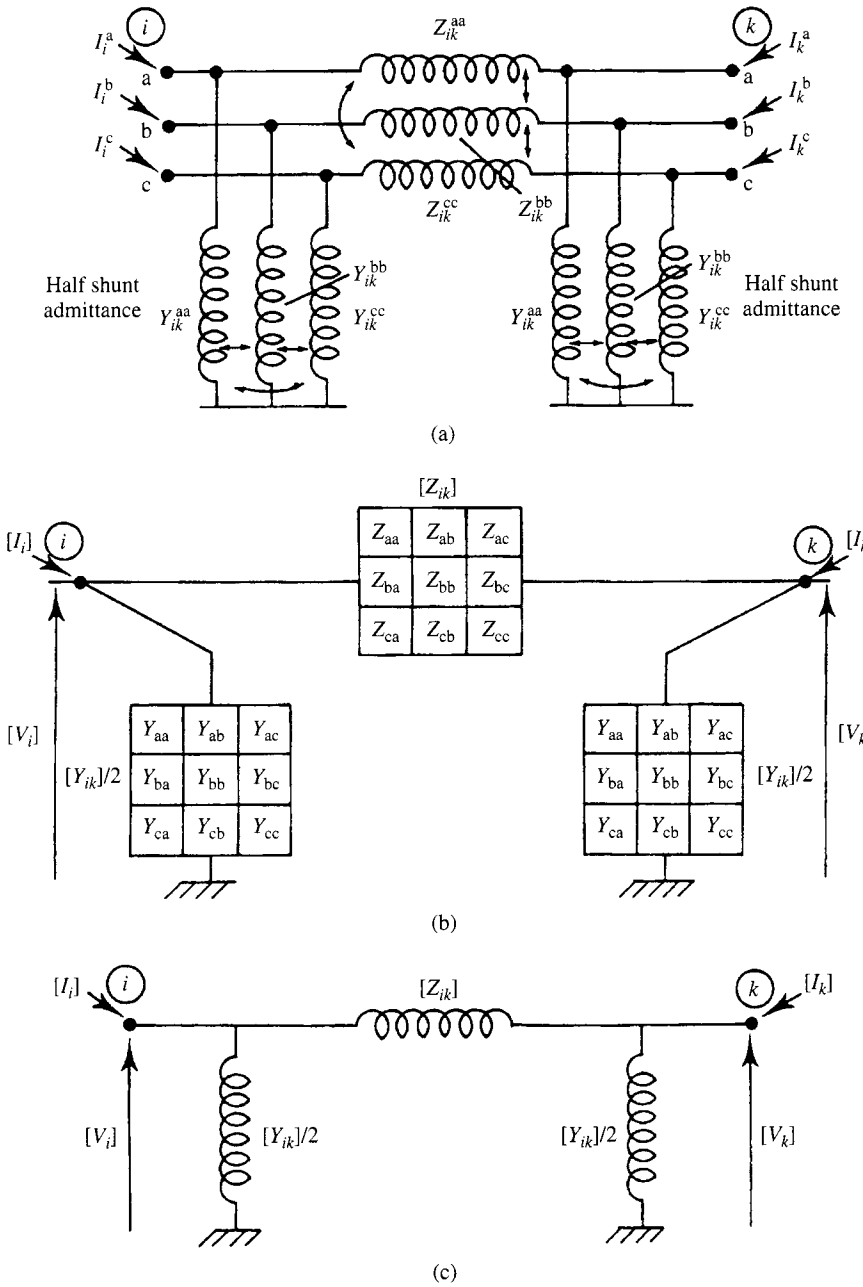

Figure 7.7 Lumped *PI* model of a short three-phase line series impedance: (a) full circuit representation; (b) matrix equivalent; (c) using three-phase compound admittances

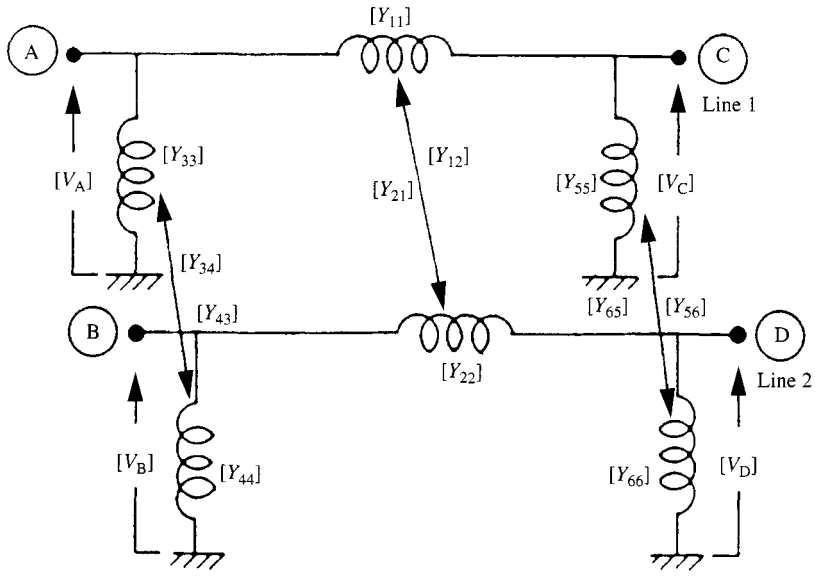

Figure 7.8 Two-coupled three-phase lines

defined as follows:

$$\begin{array}{c} \begin{bmatrix} I_A \\ I_B \\ I_C \\ I_D \end{bmatrix} \\ 12 \times 1 \end{array} = \begin{array}{c} \begin{bmatrix} Y_{11}+Y_{33} & Y_{12}+Y_{34} & -Y_{11} & -Y_{12} \\ Y_{12}^T+Y_{34}^T & Y_{22}+Y_{44} & -Y_{12}^T & -Y_{22} \\ -Y_{11} & -Y_{12} & Y_{11}+Y_{55} & Y_{12}+Y_{56} \\ -Y_{12}^T & -Y_{22} & Y_{12}^T+Y_{56}^T & Y_{22}+Y_{66} \end{bmatrix} \\ 12 \times 12 \end{array} \cdot \begin{array}{c} \begin{bmatrix} V_A \\ V_B \\ V_C \\ V_D \end{bmatrix} \\ 12 \times 1 \end{array} \tag{7.31}$$

It is assumed here that the mutual coupling is bilateral. Therefore $Y_{21} = Y_{12}^T$, etc.

The subsystem may be redrawn as in Figure 7.9. The pairs of coupled 3×3 compound admittances are now represented as a 6×6 compound admittance. The matrix representation is also shown. Following this representation and the labelling of the admittance block in the figure, the admittance matrix may be written in terms of the 6×6 compound coils as

$$\begin{array}{c} \begin{bmatrix} \begin{bmatrix} I_A \\ I_B \end{bmatrix} \\ \begin{bmatrix} I_C \\ I_D \end{bmatrix} \end{bmatrix} \\ 12 \times 1 \end{array} = \begin{array}{c} \begin{bmatrix} [Z_s]^{-1}+[Y_{s1}] & -[Z_s]^{-1} \\ -[Z_s]^{-1} & [Z_s]^{-1}+[Y_{s2}] \end{bmatrix} \\ 12 \times 12 \end{array} \begin{array}{c} \begin{bmatrix} \begin{bmatrix} V_A \\ V_B \end{bmatrix} \\ \begin{bmatrix} V_C \\ V_D \end{bmatrix} \end{bmatrix} \\ 12 \times 1 \end{array} \tag{7.32}$$

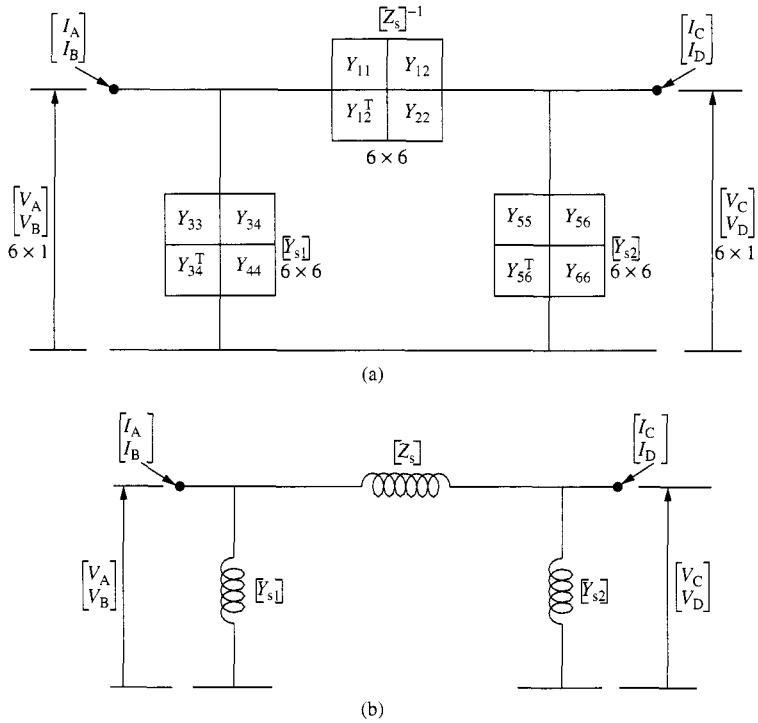

Figure 7.9 A 6 × 6 compound admittance representation of two coupled three-phase lines: (a) 6 × 6 matrix representation; (b) 6 × 6 compound admittance representation

This is clearly identical to equation (7.31) with the appropriate matrix partitioning.

The representation of Figure 7.9 is more concise and the formation of equation (7.32) from this representation is straightforward, being exactly similar to that which results from the use of 3 × 3 compound admittances for the normal single three-phase line.

The data which must be available, to enable coupled lines to be treated in a similar manner to single lines, is the series impedance and shunt admittance matrices. These matrices are of order 3 × 3 for a single line, 6 × 6 for two coupled lines, 9 × 9 for three and 12 × 12 for four coupled lines.

Once the matrices $[Z_s]$ and $[Y_s]$ are available, the admittance matrix for the subsystem is formed by application of equation (7.32).

When all the busbars of the coupled lines are distinct, the subsystem may be combined directly into the system admittance matrix. However, if the busbars are not distinct then the admittance matrix as derived from equation (7.32) must be modified. This is considered in the following section.

7.4.2 Consideration of Terminal Connections

The admittance matrix as derived above must be reduced if there are different elements in the subsystem connected to the same busbar. As an example, consider two parallel transmission lines as illustrated in Figure 7.10.

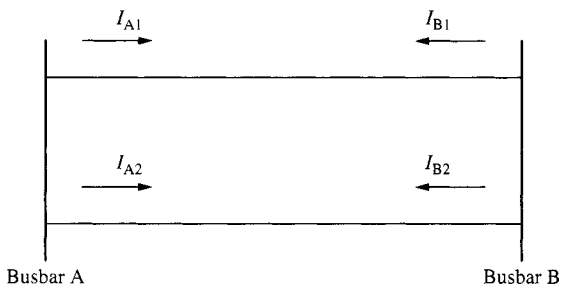

Figure 7.10 Mutually coupled parallel transmission lines

The admittance matrix derived previously related the currents and voltages at the four busbars A1, A2, B1 and B2. This relationship is given by

$$\begin{bmatrix} I_{A1} \\ I_{A2} \\ I_{B1} \\ I_{B2} \end{bmatrix} = \begin{bmatrix} \\ [Y_{A1A2B1B2}] \\ \\ \end{bmatrix} \begin{bmatrix} V_{A1} \\ V_{A2} \\ V_{B1} \\ V_{B2} \end{bmatrix} \tag{7.33}$$

The nodal injected currents at busbars A and B are given by

$$I_A = I_{A1} + I_{A2} \tag{7.34a}$$

$$I_B = I_{B1} + I_{B2} \tag{7.34b}$$

Also, from inspection of Figure 7.10

$$V_A = V_{A1} = V_{A2} \tag{7.35a}$$

$$V_B = V_{B1} = V_{B2} \tag{7.35b}$$

The required matrix equation relates the nodal injected currents, I_A and I_B, to the voltages at these busbars. This is readily derived from equation (7.33) and the conditions specified above. It is simply a matter of adding appropriate rows and columns, and yields

$$\begin{bmatrix} I_A \\ \hline I_B \end{bmatrix} = \begin{bmatrix} \\ [Y_{AB}] \\ \\ \end{bmatrix} \begin{bmatrix} V_A \\ \hline V_B \end{bmatrix} \tag{7.36}$$

where $[Y_{AB}]$ is the required nodal admittance matrix for the subsystem.

It should be noted that the matrix in equation (7.33) must be retained, as it is needed for the calculation of the individual line currents.

7.4.3 Equivalent PI Model

For long lines a number of nominal PI models are connected in series to improve the accuracy of voltages and currents, which are affected by standing wave effects.

For example, a three-section PI model provides an accuracy to 1.2% for a quarter wavelength line (a quarter wavelength corresponds to 1500 km and 1250 km at 50 Hz and 60 Hz, respectively).

As the frequency increases, the number of nominal PI sections to maintain a particular accuracy increases proportionally, e.g. a 300 km line requires 30 nominal PI sections to maintain the 1.2% accuracy for the 50th harmonic. However, near resonance the accuracy departs significantly from an acceptable value.

The computational effort can be greatly reduced and the accuracy improved with the use of an equivalent PI model derived from the solution of the second-order linear differential equations describing wave propagation along transmission lines [14]. These are:

$$\frac{d^2V(x)}{dx^2} = Z'Y'V(x) \tag{7.37a}$$

$$\frac{d^2I(x)}{dx^2} = Z'Y'I(x), \tag{7.37b}$$

where

$Z' = r + j2\pi fL$ is the series impedance per unit length and $Y' = g + j2\pi fC$ is the shunt admittance per unit length

The solution of the wave equations at a distance x from the sending end of the line is

$$V(x) = \exp(-\gamma.x)V_i + \exp(\gamma.x)V_r \tag{7.38}$$

$$I(x) = (Z')^{-1}\gamma[\exp(-\gamma.x)V_i - \exp(\gamma.x)V_r] \tag{7.39}$$

where $\gamma = \sqrt{Z'Y'} = \alpha + j\beta$ is the propagation constant, and V_i and V_r are the forward and reverse travelling voltages, respectively.

Depending on the problem in hand, e.g. if the evaluation of terminal quantities only is required, it is more convenient to formulate a solution using two-port matrix equations. This leads to the equivalent PI model, shown in Figure 7.11, where

$$Z = Z_0 \sinh(\gamma.l) \tag{7.40}$$

$$Y_1 = Y_2 = \frac{1}{Z_0}\frac{\cosh(\gamma.l) - 1}{\sinh(\gamma.l)} = \frac{1}{Z_0}\tanh\frac{(\gamma.l)}{2} \tag{7.41}$$

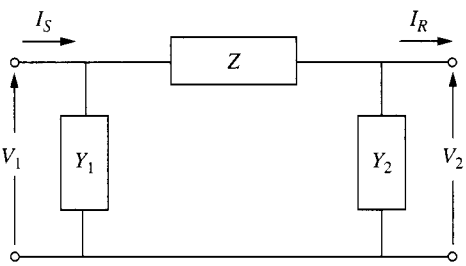

Figure 7.11 The equivalent PI model of a long transmission line

and

$$Z_0 = \sqrt{Z'/Y'} \tag{7.42}$$

is the characteristic impedance of the line.

To illustrate the characteristics of the impedances in Figure 7.11, these are plotted against frequency in Figure 7.12 for a 220 kV, 230 km line. The parameters of the line were calculated using geometric mean distances and three equal length transposition sections. The shunt resistance and shunt reactance are formed by inverting the shunt admittance.

The series and shunt reactances are the predominant components and both have a period of 1300 Hz for the test line. The line length of 230 km corresponds with one wavelength at this frequency. The series reactance increases from its inductive 50 Hz value up to a maximum at 325 Hz (the quarter wavelength frequency) and then decreases, passing through zero at 650 Hz (the half wavelength frequency). Between the half and full wavelength frequencies the series reactance is capacitive. By contrast, the shunt reactance is capacitive and large at fundamental frequency, reducing in magnitude to zero at the half wavelength frequency. Beyond this it becomes inductive.

The series resistance is small at audio frequencies. This is to be expected in a system designed to transmit power at fundamental frequency with minimum losses. Also, the peak magnitudes increase slowly as frequency increases. Since the series resistance does not get appreciably larger over the audio frequency range, the attenuation does not increase significantly. Thus, currents with frequencies in this range will propagate large distances on the power system. The negative resistances are a mathematical artifice and are not physically measurable. However they give the correct terminal conditions for a distributed parameter transmission line.

The shunt resistance, which is normally considered to be zero in a nominal PI model, has considerable effect at resonant frequencies and, as can be observed from Figure 7.12, becomes very large as the wavelength frequency is approached.

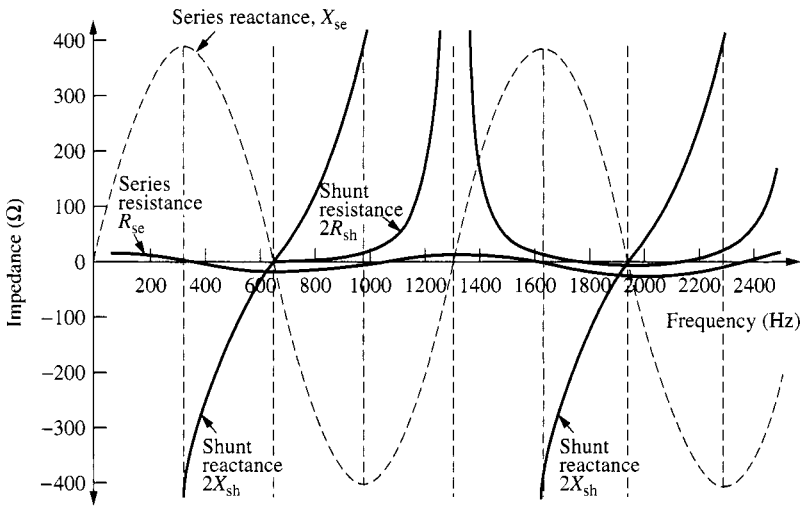

Figure 7.12 Impedance versus frequency for the equivalent PI model (skin effect included)

The impedance variation of a transmission line at resonance is similar to the case of a series and parallel resonating tuned circuit. In Figure 7.12 the series and shunt reactances are equal in magnitude but of opposite sign at 325 Hz, i.e. there is a series resonance (or node) with a low purely resistive impedance. This effect is better illustrated in Figure 7.13, where the impedance of the open circuited line is plotted. In this case the low impedance magnitude (series resonance) only contains the series and shunt resistances and occurs at the odd quarter wavelength frequencies.

At 650 Hz, although both the series and shunt reactances are small, the transmission line has a high impedance equivalent to a parallel resonating tuned circuit. This condition is called an antinode and can also be observed in Figure 7.13. The parallel resonances occur at the half wavelength frequencies.

Low impedance at the odd quarter wavelength frequencies and large impedance at the half wavelength frequencies indicate the low level of attenuation of the audio frequency signals. The addition of other system components such as loads and generators must provide the harmonic damping.

The asymptotes of Figure 7.13 are calculated from knowledge of the total series impedance, Z, and shunt admittance, Y, of the line [14]. The propagation constant γ is

$$\gamma = \sqrt{(ZY)} = \alpha + j\beta \tag{7.43}$$

where α is the attenuation constant and β is the phase constant. The characteristic impedance Z_0 is

$$Z_0 = \sqrt{(Z/Y)}$$

The upper asymptote or maximum impedance is

$$Z_0 \coth \alpha l$$

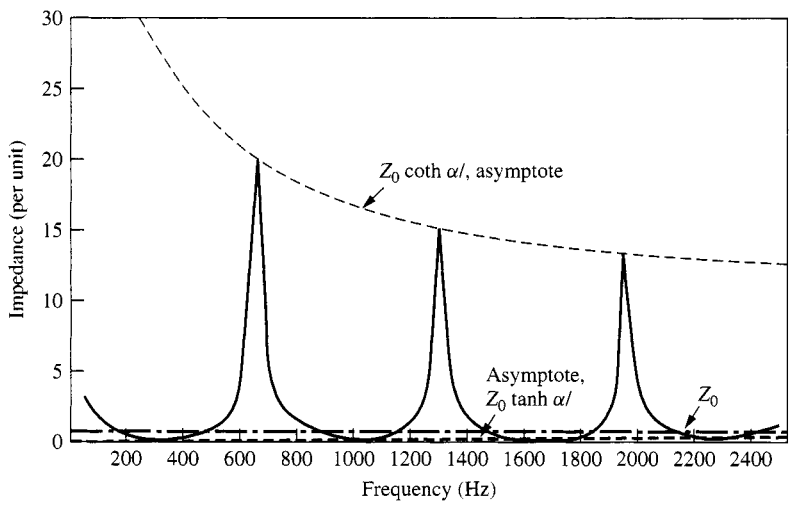

Figure 7.13 Impedance versus frequency for the open circuited Islington to Kikiwa transmission line (skin effect included)

and the lower asymptote or minimum impedance is

$$Z_0 \tanh \alpha l$$

The lower asymptote is small in value and slowly increases with frequency, while the upper asymptote decreases from an infinite value as frequency increases. For large frequencies these two asymptotes approach a value equal to the characteristic impedance.

In the case of multiconductor transmission lines, the nominal PI series impedance and shunt admittance matrices per unit distance, $[Z']$ and $[Y']$ respectively, are square and their size is fixed by the number of mutually coupled conductors.

The derivation of the equivalent PI model for harmonic penetration studies from the nominal PI matrices is similar to that of the single-phase lines, except that it involves the evaluation of hyperbolic functions of the propagation constant, which is now a matrix

$$[\gamma] = ([Z'][Y'])^{1/2} \tag{7.44}$$

There is no direct way of calculating sinh or tanh of a matrix, thus a method using eigenvalues and eigenvectors, called *modal analysis*, is employed [15] that leads to the following expressions for the series and shunt components of the equivalent PI circuit [16]:

$$[Z]_{\text{EPM}} = l[Z'][M]\left[\frac{\sinh \gamma l}{\gamma l}\right][M]^{-1} \tag{7.45}$$

where l is the transmission line length, $[Z]_{\text{EPM}}$ is the equivalent PI series impedance matrix, $[M]$ is the matrix of normalised eigenvectors,

$$\left[\frac{\sinh \gamma l}{\gamma l}\right] = \begin{bmatrix} \dfrac{\sinh \gamma_1 l}{\gamma_1 l} & 0 & \cdots & 0 \\ 0 & \dfrac{\sinh \gamma_2 l}{\gamma_2 l} & \cdots & 0 \\ \vdots & \vdots & \vdots & \\ 0 & 0 & \dfrac{\sinh \gamma_j l}{\gamma_j l} & \end{bmatrix} \tag{7.46}$$

and γ_j is the jth eigenvalue for $j/3$ mutually coupled circuits. Similarly

$$\frac{1}{2}[Y]_{\text{EPM}} = \frac{1}{2}l[M]\left[\frac{\tanh(\gamma l/2)}{\gamma l/2}\right][M]^{-1}[Y'] \tag{7.47}$$

where $[Y]_{\text{EPM}}$ is the equivalent PI shunt admittance matrix.

Computer derivation of the correction factors for conversion from the nominal PI to the equivalent PI model, and their incorporation into the series impedance and shunt admittance matrices, is carried out as indicated in the structure diagram of Figure 7.14. The LR2 algorithm of Wilkinson and Reinsch [17] is used with due regard for accurate calculations in the derivation of the eigenvalues and eigenvectors.

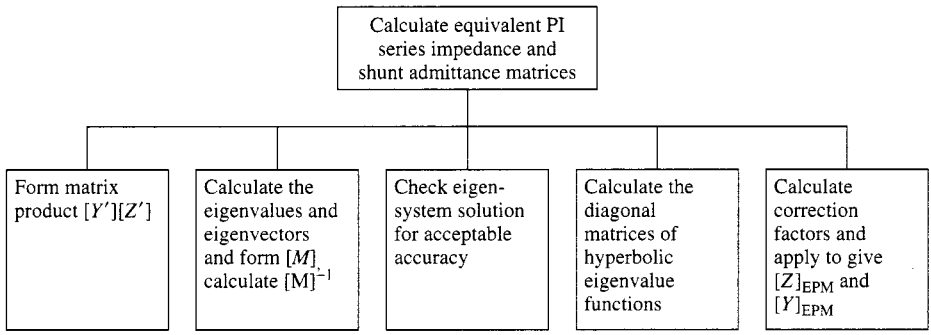

Figure 7.14 Structure diagram for calculation of the equivalent PI model

7.4.4 Evaluation of Transmission Line Parameters

The lumped series impedance matrix $[Z]$ of a transmission line consists of three components, while the shunt admittance matrix $[Y]$ contains one.

$$[Z] = [Z_e] + [Z_g] + [Z_c] \tag{7.48}$$

$$[Y] = [Y_g] \tag{7.49}$$

where $[Z_c]$ is the internal impedance of the conductors ($\Omega \cdot \text{km}^{-1}$), $[Z_g]$ is the impedance due to the physical geometry of the conductor's arrangement ($\Omega \cdot \text{km}^{-1}$), $[Z_e]$ is the earth return path impedance ($\Omega \cdot \text{km}^{-1}$), and $[Y_g]$ is the admittance due to the physical geometry of the conductor ($\Omega^{-1} \cdot \text{km}^{-1}$).

In multiconductor transmission all *primitive matrices* (the admittance matrices of the unconnected branches of the original network components) are symmetric and, therefore, the functions that define the elements need only be evaluated for elements on or above the leading diagonal.

Earth Impedance Matrix [Z_e] The impedance due to the earth path varies with frequency in a nonlinear fashion. The solution of this problem, under idealised conditions, has been given in the form of either an infinite integral or an infinite series [18].

As the need arises to calculate ground impedances for a wide spectrum of frequencies, the tendency is to select simple formulations aiming at a reduction in computing time, while maintaining a reasonable level of accuracy.

Consequently, what was originally a heuristic approach [19] is becoming the more favoured alternative, particularly at high frequencies.

Based on Carson's work, the ground impedance can be concisely expressed as

$$Z_e = 1000 J(r, \theta)(\Omega \cdot \text{km}^{-1}) \tag{7.50}$$

where

$$Z_e \in [Z_e]$$

$$J(r, \theta) = \frac{\omega \mu_a}{\pi}\{P(r, \theta) + jQ(r, \theta)\}$$

$$r_{ij} = \sqrt{\frac{\omega\mu_a}{\rho}}\ D_{ij}$$

$$D_{ij} = \sqrt{(h_i + h_j)^2 + d^2{}_{ij}} \qquad \text{for } i \neq j$$

$$D_{ij} = 2h_i \qquad \text{for } i = j$$

$$\theta_{ij} = \arctan \frac{d_{ij}}{h_i + h_j} \qquad \text{for } i \neq j$$

$$\theta_{ij} = 0 \qquad \text{for } i = j$$

$\omega = 2\pi f (\text{rad} \cdot \text{s}^{-1})$

f is frequency (Hz)

h_i is the height of conductor i (m)

d_{ij} is the horizontal distance between conductors i and j (m)

μ_a is the permeability of free space $= 7\pi \times 10^{-7} (\text{H} \cdot \text{m}^{-1})$

ρ is the earth resistivity $(\Omega \cdot \text{m})$.

Carson's solution to equation (7.50) is defined by eight different infinite series which converge quickly for problems related to transmission line parameter calculation, but the number of required computations increases with frequency and separation of the conductors.

More recent literature has described closed form formulations for the numerical evaluation of line-ground loops, based on the concept of a mirroring surface beneath the earth at a certain depth. The most popular complex penetration model, which has had more appeal is that of C. Dubanton [20], due to its simplicity and high degree of accuracy for the whole frequency span for which Carson's equations are valid.

Dubanton's formulae for the evaluation of the self- and mutual impedances of conductors i and j are

$$Z_{ii} = \frac{j\omega\mu_o}{2\pi} \times \ln \frac{2(h_i + p)}{r_i} \tag{7.51}$$

$$Z_{ij} = \frac{j\omega\mu_o}{2\pi} \times \ln \frac{\sqrt{2(h_i + p)}}{\sqrt{(h_i - h_j)^2 + d^2{}_{ij}}} \tag{7.52}$$

where $p = 1/\sqrt{j\omega\mu_o\sigma}$ is the complex depth below the earth at which the mirroring surface is located.

An alternative and very simple formulation has been proposed [21], which for the purpose of harmonic penetration yields accurate solutions when compared to those obtained using Carson's equations.

Geometrical Impedance Matrix $[Z_g]$ and Admittance Matrix $[Y_g]$ If the conductors and the earth are assumed to be equipotential surfaces, the geometrical impedance can be formulated in terms of potential coefficients theory.

The self-potential coefficient ψ_{ii} for the ith conductor and the mutual potential coefficient ψ_{ij} between the ith and jth conductors are defined as follows:

$$\psi_{ii} = \ln(2h_i/r_i) \tag{7.53}$$

$$\psi_{ij} = \ln(\mathrm{D}_{ij}/d_{ij}) \tag{7.54}$$

where r_i is the radius of the ith conductor (m) while the other variables are as defined earlier.

Potential coefficients depend entirely on the physical arrangement of the conductors and need only be evaluated once.

For practical purposes the air is assumed to have zero conductance and

$$[Z_g] = j\omega \mathrm{K}'[\psi]\ \Omega/\mathrm{km} \tag{7.55}$$

where $[\psi]$ is a matrix of potential coefficients and $\mathrm{K}' = 2 \times 10^{-4}$.

The lumped shunt admittance parameters [**Y**] are completely defined by the inverse relation of the potential coefficients matrix, i.e.

$$[Y_g] = 1000 j\omega 2\pi \varepsilon_a [\psi]^{-1} \tag{7.56}$$

where ε_a is permittivity of free space $= 8.857 \times 10^{-12}$ $(\mathrm{F} \cdot \mathrm{m}^{-1})$.

As $[Z_g]$ and $[Y_g]$ are linear functions of frequency, they need only be evaluated once and scaled for other frequencies.

Conductor Impedance Matrix [Z_c] This term accounts for the internal impedance of the conductors. Both resistance and inductance have a nonlinear frequency dependence. Current tends to flow on the surface of the conductor, the *skin effect,* which increases with frequency and needs to be computed at each frequency. An accurate result for a homogeneous nonferrous conductor of annular cross-section involves the evaluation of long equations based on the solution of Bessel functions, as shown in equation (7.57).

$$\mathrm{Z_c} = \frac{j\omega\mu_o}{2\pi} \frac{1}{x_e} \frac{\mathrm{J_o}(x_e)\mathrm{N}'_o(x_i) - \mathrm{N_o}(x_e)\mathrm{J}'_o(x_i)}{\mathrm{J}'_o(x_e)\mathrm{N}'_o(x_i) - \mathrm{N}'_o(x_e)\mathrm{J}'_o(x_i)} \tag{7.57}$$

where

$x_e = j\sqrt{j\omega\mu_o\sigma_c}r_e$
$x_i = j\sqrt{j\omega\mu_o\sigma_c}r_i$
r_e is the external radius of the conductor (m)
r_i is the internal radius of the conductor (m)
$\mathrm{J_o}$ is the Bessel function of the first kind and zero order
J'_o is the derivative of the Bessel function of the first kind and zero order
$\mathrm{N_o}$ is the Bessel function of the second kind and zero order
N'_o is the derivative of the Bessel function of the second kind and zero order
σ_c is the conductivity of the conductor material at the average conductor temperature.

The Bessel functions and their derivatives are solved, within a specified accuracy, by means of their associated infinite series. Convergence problems are frequently encountered at high frequencies and low ratios of conductor thickness to external radius i.e. $(r_e - r_i)/r_e$, necessitating the use of asymptotic expansions.

A new closed form solution has been proposed [19] based on the concept of complex penetration; unfortunately errors of up to 6.6% occur in the region of interest.

To overcome the difficulties of slow convergence of the Bessel function approach and the inaccuracy of the complex penetration method at relatively low frequencies, an alternative approach based upon curve fitting to the Bessel function formula has been proposed [21].

For long lines, skin effect resistance (R_{ac}/R_{dc}) ratios and their effect on the resonant voltage magnitudes are important. Because the series resistance of a transmission line is a small component of the series impedance when the transmission line is not at resonance, the harmonic voltages, shown in Figure 7.15, do not change to any significant extent when skin effect is included. At resonance the series resistance and shunt conductance become the dominant system components. Changes in the series resistance magnitude change the voltage peaks but do not affect the resonance frequency.

In Figure 7.15 the voltage calculated with skin effect is, at resonance, 50% higher than without skin effect; these results correspond with an R_{ac}/R_{dc} ratio of 2. In a single-phase model without ground return the ratio of voltages at resonance, with and without skin effect, is the same as the skin effect ratio. In a three-phase model the presence of shunt conductance and series resistance coupling between phases, and the different resonant frequencies of the phases, reduces the resonant peak voltages compared with single-phase modelling.

Skin effect is also taken into account in modelling the earth return as a conductor. The depth of penetration of the earth currents decreases with an increase in frequency or a decrease in earth resistivity. The series inductance decreases as a result of these changes.

As an alternative to the rigorous analysis described above, power companies often use approximations to the skin effect by means of correction factors. Typical corrections in current use by the NGC (UK) and EDF (France) are given in Table 7.1.

Lewis and Tuttle [22] presented a practical method for calculating the skin effect resistance ratio by approximating ACSR (aluminium conductor steel reinforced)

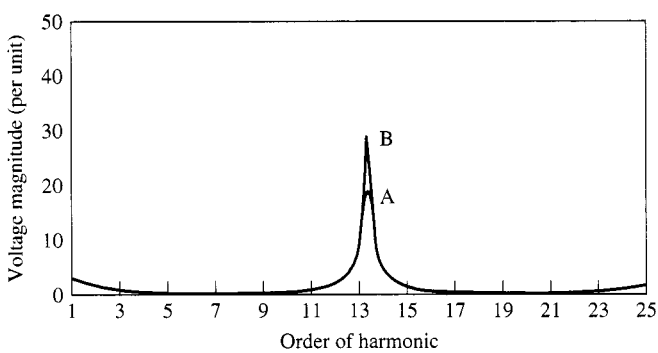

Figure 7.15 The result of modelling: curve A, skin effect included; curve B, no skin effect

Table 7.1 Corrections for skin effect in overhead lines

Company	Voltage (kV)	Harmonic order	Resistance
NGC	400, 275 (based on 0.4 sq.in. steel-core al. conductors)	$h \leq 4.21$	$R_1\left(1+\dfrac{3.45h^2}{192+2.77h^2}\right)$
	132	$4.21 < h \leq 7.76$	$R_1(0.806+0.105h)$
		$h > 7.76$	$R_1(0.267+0.485\sqrt{h})$
			$R_1\left(1+\dfrac{0.6465h^2}{192+0518h^2}\right)$
EDF	400, 225	$h \leq 4$	$R_1\left(1+\dfrac{3.45h^2}{192+2.77h^2}\right)$
		$4 < h < 8$	$R_1(0.864-0.024\sqrt{h}+0.105h)$
		$8 < h$	$R_1(0.267+0.485\sqrt{h})$
	150, 90		$R_1\left(1+\dfrac{0.646h^2}{192+0.518h^2}\right)$

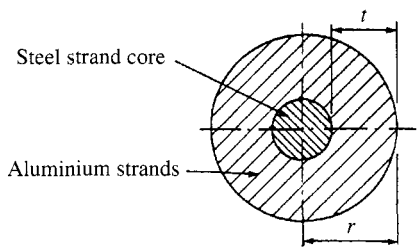

Figure 7.16 ACSR hollow tube conductor representation

conductors to uniform tubes having the same inside and outside diameters as the aluminium conductors (Figure 7.16). Figure 7.17 illustrates the skin effect ratio for different models and various tube ratios for ACSR conductors. Skin effect modelling is important for long lines. Although the series resistance of a transmission line is typically a small component of the series impedance, it dominates its value at resonances.

7.5 Underground and Submarine Cables [23]

A unified solution similar to that of overhead transmission is difficult for underground cables because of the great variety in their construction and layouts.

The cross-section of a cable, although extremely complex, can be simplified to that of Figure 7.18 and its series per unit length harmonic impedance is calculated by the

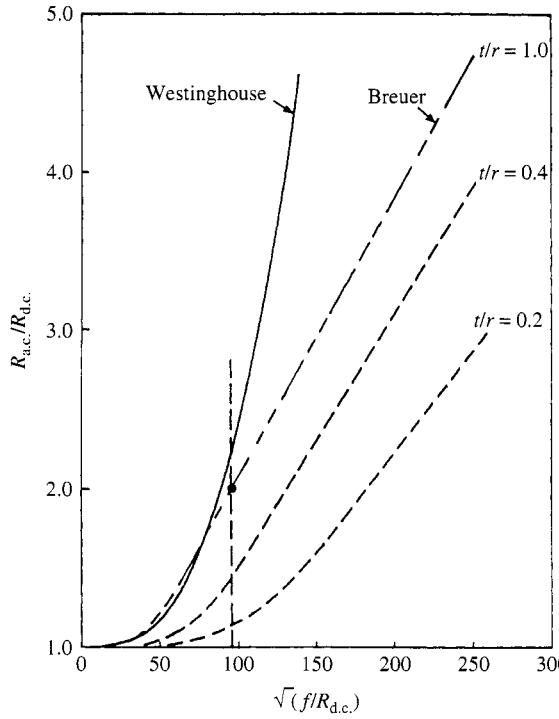

Figure 7.17 Skin effect resistance for different models

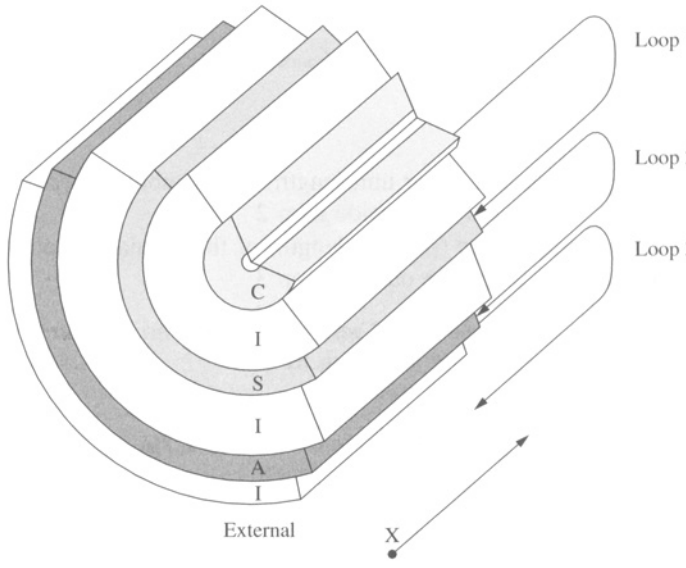

Figure 7.18 Cable cross-section

following set of loop equations.

$$-\begin{bmatrix} dV_1/dx \\ dV_2/dx \\ dV_3/dx \end{bmatrix} = \begin{bmatrix} Z'_{11} & Z'_{12} & 0 \\ Z'_{21} & Z'_{22} & Z'_{23} \\ 0 & Z'_{32} & Z'_{33} \end{bmatrix} \begin{bmatrix} I_1 \\ I_2 \\ I_3 \end{bmatrix} \tag{7.58}$$

where Z'_{11} is the sum of the following three component impedances:

$Z'_{\text{core-outside}}$: internal impedance of the core with the return path outside the core

$Z'_{\text{core-insulation}}$: impedance of the insulation surrounding the core

$Z'_{\text{sheath-inside}}$: internal impedance of the sheath with the return path inside the sheath.

Similarly

$$Z'_{22} = Z'_{\text{sheath-outside}} + Z'_{\text{sheath/armour-insulation}} + Z'_{\text{armour-inside}} \tag{7.59}$$

and

$$Z'_{33} = Z'_{\text{armour-outside}} + Z'_{\text{armour/earth-insulation}} + Z'_{\text{earth-inside}} \tag{7.60}$$

The coupling impedances $Z'_{12} = Z'_{21}$ and $Z'_{23} = Z'_{32}$ are negative because of opposing current directions (I_2 in negative direction in loop 1, and I_3 in negative direction in loop 2), i.e.

$$Z'_{12} = Z'_{21} = -Z'_{\text{sheath-mutual}} \tag{7.61}$$

$$Z'_{23} = Z'_{32} = -Z'_{\text{armour-mutual}} \tag{7.62}$$

where

$Z'_{\text{sheath-mutual}}$: mutual impedance (per unit length) of the tubular sheath between inside loop 1 and the outside loop 2

$Z'_{\text{armour-mutual}}$: mutual impedance (per unit length) of the tubular armour between the inside loop 2 and the outside loop 3

Finally, $Z'_{13} = Z'_{31} = 0$ because loop 1 and loop 3 have no common branch.

The impedances of the insulation are given by

$$Z'_{\text{insulation}} = j\omega \frac{\mu}{2\pi} \ln \frac{r_{\text{outside}}}{r_{\text{inside}}} \quad \text{in } \Omega/m \tag{7.63}$$

where μ is the permeability of insulation in H/m, r_{outside} is the outside radius of insulation and r_{inside} is the inside radius of insulation.

If there is no insulation between the armour and earth, then Z' insulation $= 0$.

The internal impedances and the mutual impedance of a tubular conductor are a function of frequency, and can be derived from Bessel and Kelvin functions.

$$Z'_{\text{tube-inside}} = \frac{\sqrt{j}.\omega.\mu}{2\pi.mq.D}[I_o(\sqrt{j}mq)K_1(\sqrt{j}mr) + K_o(\sqrt{j}mq)I_1(\sqrt{j}mr)] \tag{7.64}$$

$$Z'_{\text{tube-outside}} = \frac{\sqrt{j}.\omega.\mu}{2\pi.mr.D}[I_o(\sqrt{j}mr)K_1(\sqrt{j}mq) + K_o(\sqrt{j}mr)I_1(\sqrt{j}mq)] \tag{7.65}$$

$$Z'_{\text{tube-mutual}} = \frac{\omega.\mu}{2\pi.mq.mr.D} \tag{7.66}$$

with

$$D = I_1(\sqrt{j}mr)K_1(\sqrt{j}mq) - I_1(\sqrt{j}mq)K_1(\sqrt{j}mr) \tag{7.67}$$

where

$$mr = \sqrt{K\frac{1}{1-s^2}} \tag{7.68}$$

$$mq = \sqrt{K\frac{s^2}{1-s^2}} \tag{7.69}$$

with

$$K = \frac{8\pi.10^{-4}.f.\mu_r}{R'_{\text{dc}}} \tag{7.70}$$

$$s = \frac{q}{r} \tag{7.71}$$

where q is the inside radius, r is the outside radius and R'_{dc} is the d.c. resistance in Ω/Km.

The only remaining term is $Z'_{\text{earth-inside}}$ in equation (7.60), which is the earth return impedance for underground cables, or the sea return impedance for submarine cables. The earth return impedance can be calculated approximately with equation (7.64) by letting the outside radius go to infinity. This approach, also used by Bianchi and Luoni [24] to find the sea return impedance, is quite acceptable considering the fact that sea resistivity and other input parameters are not known accurately.

Equation (7.58) is not in a form compatible with the solution used for overhead conductors, where the voltages with respect to local ground and the actual currents in the conductors are used as variables. Equation (7.58) can easily be brought into such a form by introducing the appropriate terminal conditions, namely with

$$\begin{aligned} V_1 &= V_{\text{core}} - V_{\text{sheath}} & I_1 &= I_{\text{core}} \\ V_2 &= V_{\text{sheath}} - V_{\text{armour}} & I_2 &= I_{\text{core}} + I_{\text{sheath}} \\ V_3 &= V_{\text{armour}} & I_3 &= I_{\text{core}} + I_{\text{sheath}} + I_{\text{armour}} \end{aligned}$$

Equation (7.58) can be rewritten as

$$-\begin{bmatrix} dV_{\text{core}}/dx \\ dV_{\text{sheath}}/dx \\ dV_{\text{armour}}/dx \end{bmatrix} = \begin{bmatrix} Z'_{\text{cc}} & Z'_{\text{cs}} & Z'_{\text{ca}} \\ Z'_{\text{sc}} & Z'_{\text{ss}} & Z_{\text{sa}} \\ Z'_{\text{ac}} & Z'_{\text{as}} & Z'_{\text{aa}} \end{bmatrix} \begin{bmatrix} I_{\text{core}} \\ I_{\text{sheath}} \\ I_{\text{armour}} \end{bmatrix} \tag{7.72}$$

where

$$
\begin{aligned}
Z'_{cc} &= Z'_{11} + 2Z'_{12} + Z'_{22} + 2Z'_{23} + Z'_{33} \\
Z'_{cs} &= Z'_{sc} = Z'_{12} + Z'_{22} + 2Z'_{23} + Z'_{33} \\
Z'_{ca} &= Z'_{ac} = Z'_{sa} = Z'_{as} = Z'_{23} + Z'_{33} \\
Z'_{ss} &= Z'_{22} + 2Z'_{23} + Z'_{33} \\
Z'_{aa} &= Z'_{33}
\end{aligned}
$$

Because a good approximation for many cables having bonding between the sheath and the armour, and the armour earthed to the sea, is $V_{\text{sheath}} = V_{\text{armour}} = 0$, the system can be reduced to

$$-\mathrm{d}V_{\text{core}}/\mathrm{d}x = ZI_{\text{core}} \tag{7.73}$$

where Z is a reduction of the impedance matrix of equation (7.72).

Similarly, for each cable the per unit length harmonic admittance is

$$-\begin{bmatrix} \mathrm{d}I_1/\mathrm{d}x \\ \mathrm{d}I_2/\mathrm{d}x \\ \mathrm{d}I_3/\mathrm{d}x \end{bmatrix} = \begin{bmatrix} j\omega C'_1 & 0 & 0 \\ 0 & j\omega C'_2 & 0 \\ 0 & 0 & j\omega C'_3 \end{bmatrix} \begin{bmatrix} V_1 \\ V_2 \\ V_3 \end{bmatrix} \tag{7.74}$$

where $C'_i = 2\pi\varepsilon_0\varepsilon_r / l_n(r/q)$. Therefore, when converted to core, sheath and armour quantities,

$$-\begin{bmatrix} \mathrm{d}I_{\text{core}}/\mathrm{d}x \\ \mathrm{d}I_{\text{sheath}}/\mathrm{d}x \\ \mathrm{d}I_{\text{armour}}/\mathrm{d}x \end{bmatrix} = \begin{bmatrix} Y'_1 & -Y'_1 & 0 \\ -Y'_1 & Y' + Y'_2 & -Y'_2 \\ 0 & -Y'_2 & Y'_2 + Y'_3 \end{bmatrix} \begin{bmatrix} V_{\text{core}} \\ V_{\text{sheath}} \\ V_{\text{armour}} \end{bmatrix} \tag{7.75}$$

where $Y'_i = j\omega l_i$. If, as before, $V_{\text{sheath}} = V_{\text{armour}} = 0$, equation (7.75) reduces to

$$-\mathrm{d}I_{\text{core}}\mathrm{d}x = Y'_1 V_{\text{core}} \tag{7.76}$$

Therefore, for frequencies of interest, the cable per unit length harmonic impedance, Z', and admittance, Y', are calculated with both the zero- and positive-sequence values being equal to the Z in equation (7.73), and the Y' in equation (7.76), respectively.

In the absence of rigorous computer models, such as described above, power companies often use approximations to the skin effect by means of correction factors. Typical corrections used by the NGC (UK) and EDF (France) are given in Table 7.2.

7.6 Three-Phase Transformer Models

The basic three-phase two-winding transformer is shown in Figure 7.19. Its primitive network, on the assumption that the flux paths are symmetrically distributed between

Table 7.2 Corrections for skin effect in cables

Company	Voltage (kV)	Harmonic order	Resistance
NGC	400, 275 (based on 2.5 sq.in. conductor at 5 in. spacing between centres)	$h \geq 1.5$	$0.74\ R_1\ (0.267 + 1.073\sqrt{h})$
	132	$h \geq 2.35$	$R_1\ (0.187 + 0.532\sqrt{h})$
EDF	400, 225	$h \geq 2$	$0.74\ R_1\ (0.267 + 1.073\sqrt{h})$
	150, 90	$h \geq 2$	$R_1\ (0.187 + 0.532\sqrt{h})$

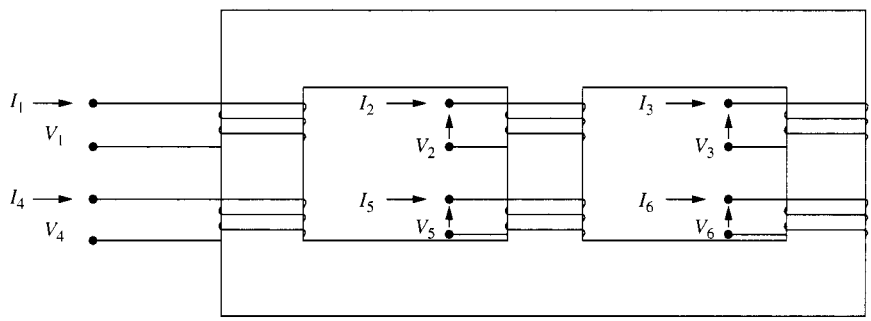

Figure 7.19 Diagrammatic representation of a two-winding transformer

all windings, is represented by the equation

$$\begin{bmatrix} I_1 \\ I_2 \\ I_3 \\ I_4 \\ I_5 \\ I_6 \end{bmatrix} = \begin{bmatrix} y_p & y'_m & y'_m & -y_m & y''_m & y''_m \\ y'_m & y_p & y'_m & y''_m & -y_m & y''_m \\ y'_m & y'_m & y_p & y''_m & y''_m & -y_m \\ -y_m & y''_m & y''_m & y_s & y'''_m & y'''_m \\ y''_m & -y_m & y''_m & y'''_m & y_s & y'''_m \\ y''_m & y''_m & -y_m & y'''_m & y'''_m & y_s \end{bmatrix} \begin{bmatrix} V_1 \\ V_2 \\ V_3 \\ V_4 \\ V_5 \\ V_6 \end{bmatrix} \tag{7.77}$$

where y'_m is the mutual admittance between primary coils, y''_m is the mutual admittance between primary and secondary coils on different cores, and y'''_m is the mutual admittance between secondary coils.

If a tertiary winding is also present, the primitive network consists of nine (instead of six) coupled coils and its mathematical model will be a 9×9 admittance matrix.

The interphase coupling can usually be ignored (e.g. the case of three single-phase separate units) and all the primed terms are effectively zero.

The connection matrix $[C]$ between the primitive network and the actual transformer buses is derived from the transformer connection.

By way of example, consider the Wye G-Delta connection of Figure 7.20. The following connection matrix applies:

$$\begin{bmatrix} V_1 \\ V_2 \\ V_3 \\ V_4 \\ V_5 \\ V_6 \end{bmatrix} = \begin{bmatrix} 1 & 0 & 0 & 0 & 0 & 0 \\ 0 & 1 & 0 & 0 & 0 & 0 \\ 0 & 0 & 1 & 0 & 0 & 0 \\ 0 & 0 & 0 & 1 & -1 & 0 \\ 0 & 0 & 0 & 0 & 1 & -1 \\ 0 & 0 & 0 & -1 & 0 & 1 \end{bmatrix} \begin{bmatrix} V_p^a \\ V_p^b \\ V_p^c \\ V_s^A \\ V_s^B \\ V_s^C \end{bmatrix} \tag{7.78}$$

or

$$[V]_{\text{Branch}} = [C]\,[V]_{\text{node}} \tag{7.79}$$

We can also write

$$[Y]_{\text{NODE}} = [C]^{\text{T}}[Y]_{\text{PRIM}}[C] \tag{7.80}$$

and using $[Y]_{\text{PRIM}}$ from equation (7.77)

$[Y]_{\text{NODE}} =$

y_p	y'_m	y'_m	$-(y_m + y''_m)$	$(y_m + y''_m)$	0	A
y'_m	y_p	y'_m	0	$-(y_m + y''_m)$	$(y_m + y''_m)$	B
y'_m	y'_m	y_p	$(y_m + y''_m)$	0	$-(y_m + y''_m)$	C
$-(y_m + y''_m)$	0	$(y_m + y''_m)$	$2(y_s - y'''_m)$	$-(y_s - y'''_m)$	$-(y_s - y'''_m)$	A
$(y_m + y''_m)$	$-(y_m + y''_m)$	0	$-(y_s - y'''_m)$	$2(y_s - y'''_m)$	$-(y_s - y'''_m)$	B
0	$(y_m + y''_m)$	$-(y_m + y''_m)$	$-(y_s - y'''_m)$	$-(y_s - y'''_m)$	$2(y_s - y'''_m)$	C

(7.81)

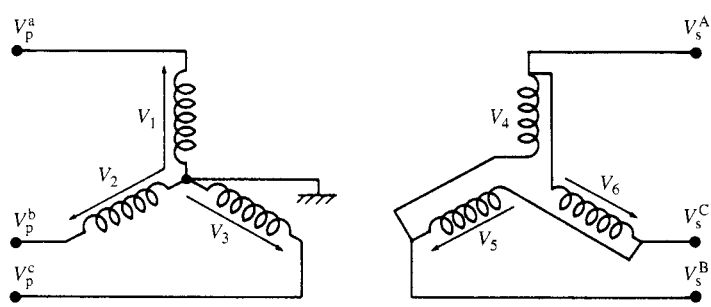

Figure 7.20 Network connection diagram for a Wye G-delta transformer

If the primitive admittances are expressed in per unit the upper-right and lower-left quadrants of matrix (7.81) must be divided by $\sqrt{3}$ and the lower-right quadrant by 3. Then, in the absence of interphase coupling, the nodal admittance matrix equation of the Wye G-delta connection becomes

$$\begin{bmatrix} I_p^a \\ I_p^b \\ I_p^c \\ I_s^A \\ I_s^B \\ I_s^C \end{bmatrix} = \begin{bmatrix} y & & & -y/\sqrt{3} & y/\sqrt{3} & \\ & y & & & -y/\sqrt{3} & y/\sqrt{3} \\ & & y & y/\sqrt{3} & & -y/\sqrt{3} \\ -y/\sqrt{3} & & y/\sqrt{3} & 2/3y & -1/3y & -1/3y \\ y/\sqrt{3} & -y/\sqrt{3} & & -1/3y & 2/3y & -1/3y \\ & y/\sqrt{3} & -y/\sqrt{3} & -1/3y & -1/3y & 2/3y \end{bmatrix} \begin{bmatrix} V_p^a \\ V_p^b \\ V_p^c \\ V_s^A \\ V_s^B \\ V_s^C \end{bmatrix} \tag{7.82}$$

where y is the transformer leakage admittance in per unit, which is approximated by

$$Y_{th} = \frac{1}{R\sqrt{h} + jX_1 h} \tag{7.83}$$

where R is the resistance at fundamental frequency and X_l is the transformer's leakage reactance.

An example of a typical variation of the inductive coefficient of a transformer with frequency is shown in Figure 7.21.

The magnetising admittance is usually ignored since under normal operating conditions its contribution is not significant. If, however, the transformer is under severe saturation, appropriate current harmonic sources must be added at the transformer terminals.

In general, any two-winding three-phase transformer may be represented by two coupled compound coils as shown in Figure 7.22 where $[Y_{sp}] = [Y_{ps}]^T$.

If the parameters of the three phases are assumed balanced, all the common three-phase connections can be modelled by three basic submatrices. The submatrices $[Y_{pp}]$, $[Y_{ps}]$, etc. are given in Table 7.3 for the common connections in terms of the following matrices:

$$Y_1 = \begin{bmatrix} y_t & & \\ & y_t & \\ & & y_t \end{bmatrix} \quad Y_{11} = \begin{bmatrix} 2y_t & -y_t & -y_t \\ -y_t & 2y_t & -y_t \\ -y_t & -y_t & 2y_t \end{bmatrix} \quad Y_{111} = \begin{bmatrix} -y_t & y_t & \\ & -y_t & y_t \\ y_t & & -y_t \end{bmatrix}$$

For transformers with neutrals connected through an impedance, an extra coil is added to the primitive network for each unearthed neutral and the primitive admittance increases in dimension. However, by noting that the injected current in the neutral is

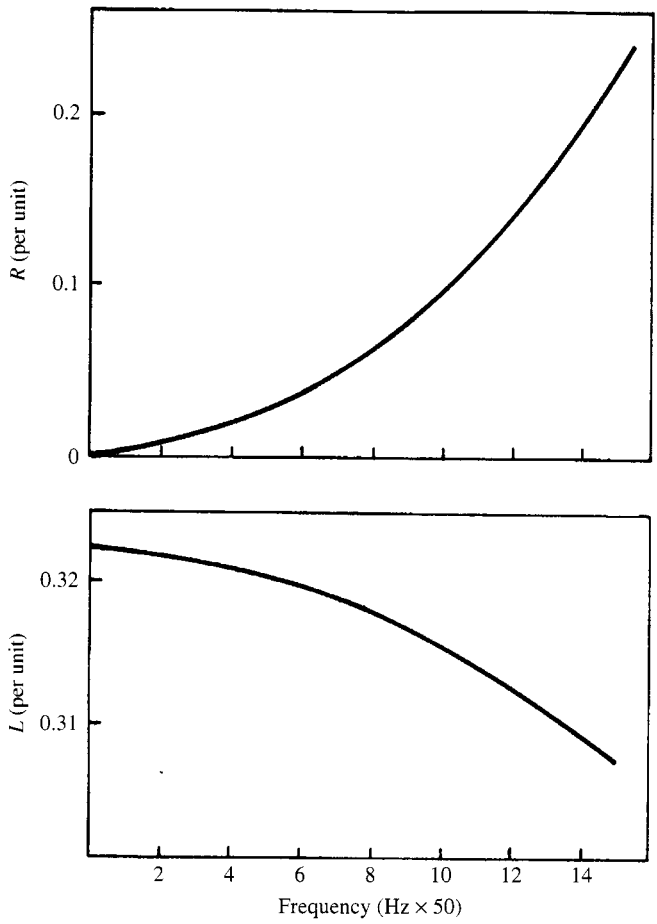

Figure 7.21 Transformer parameter frequency dependency

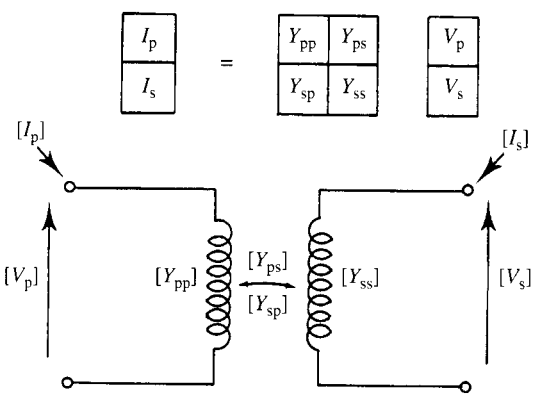

Figure 7.22 Two-winding three-phase transformer

Table 7.3 Characteristic submatrices used in forming the transformer admittance matrices

Transformer connection		Self-admittance		Mutual admittance
Bus P	Bus S	Y_{pp}	Y_{ss}	Y_{ps}, Y_{sp}
Wye G	Wye G	Y_1	Y_1	$-Y_1$
Wye G	Wye	Y_1	$Y_{11/3}$	$-Y_{11/3}$
Wye G	Delta	Y_1	Y_{11}	Y_{111}
Wye	Wye	$Y_{11/3}$	$Y_{11/3}$	$-Y_{11/3}$
Wye	Delta	$Y_{11/3}$	Y_{11}	Y_{111}
Delta	Delta	Y_{11}	Y_{11}	$-Y_{11}$

zero (no direct connection), these extra terms can be eliminated from the connected network admittance matrix. This results in the matrix:

$$Y = \begin{array}{|c|c|c|} \hline y_t - c & -c & -c \\ \hline -c & y_t - c & -c \\ \hline -c & -c & y_t - c \\ \hline \end{array} \quad \text{where } c = y_t.y_t/(3.y_t + y_n)$$

Once the admittance matrix has been formed for a particular connection it represents a simple subsystem composed of the two busbars interconnected by the transformer.

7.7 Generator Modelling

For the purpose of determining the network harmonic admittances, the generators can be modelled as a series combination of resistance and inductive reactance, i.e.

$$Y_{gh} = \frac{1}{R\sqrt{h} + jX''_d h} \tag{7.84}$$

where R is derived from the machine power losses and X''_d is the generator's sub-transient reactance.

A frequency-dependent multiplying factor can be added to the reactance terms to account for skin effect. It should be noted that equation (7.84) is not valid at fundamental frequency as the positive sequence component still sees the synchronous impedance due to the flux not rotating with respect to the rotor.

7.8 Shunt Elements

Shunt reactors and capacitors are used in a transmission system for reactive power control. The data for these elements is usually given in terms of their rated megavolt-amps and rated kilovolts, and the equivalent phase admittance in per unit is calculated from this data.

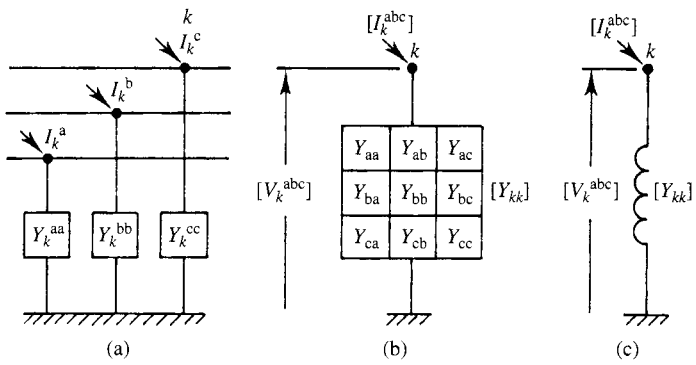

Figure 7.23 Representation of a shunt element: (a) coupled admittance; (b) admittance matrix; (c) compound admittance

The coupled admittances to ground at bus k are formed into a 3×3 admittance matrix as shown in Figure 7.23, and this reduces to the compound admittance representation indicated. The admittance matrix is incorporated directly into the system admittance matrix, contributing only to the self-admittance of the particular bus.

While provision for off-diagonal terms exists, the admittance matrix for shunt elements is usually diagonal, as there is normally no coupling between the components of each phase.

Consider, as an example, the three-phase capacitor bank shown in Figure 7.24. A 3×3 matrix representation similar to that for a line section is illustrated.

The megavolt-amp rating at fundamental frequency (Q) and the nominal voltage (V) are normally used to calculate the capacitive reactance at the n harmonic, i.e. $X_c = V^2/nQ$.

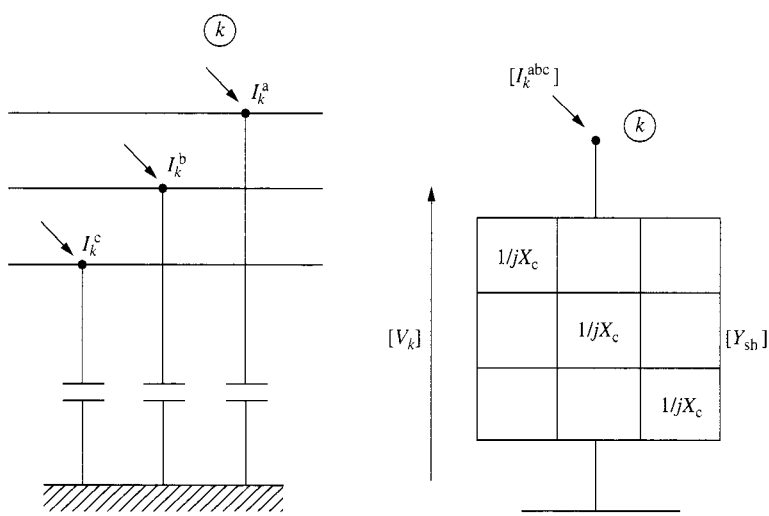

Figure 7.24 Representation of a shunt capacitor bank

In terms of *ABCD* parameters the matrix equation of a shunt element is:

$$\begin{bmatrix} V_s \\ I_s \end{bmatrix} = \begin{bmatrix} [U] & \\ [Y_{sh}] & [U] \end{bmatrix} \times \begin{bmatrix} V_r \\ -I_r \end{bmatrix} \tag{7.85}$$

where $[Y_{sh}]$ = Diag (shunt admittance of each phase) and $[U]$ = Identity matrix.

However, in harmonic analysis, any added inductance, often placed in series with shunt capacitors, must be explicitly represented. For floating star or delta-connected configurations, the procedure used in Section 7.6. for the transformer representation should be followed.

7.9 Series Elements

Series elements are connected directly between two buses and for modelling purposes they constitute a subsystem in the network subdivision.

A three-phase coupled series admittance between two busbars i and k is shown in Figure 7.25(a), as well as its reduced nodal admittance matrix (Figure 7.25(b)) and compound admittance (Figure 7.25(c)).

The series capacitor, used for transmission line reactance compensation, is an example of an uncoupled series element; in this case the admittance matrix is diagonal. For a lumped series element, the *ABCD* parameter matrix equation is:

$$\begin{bmatrix} V_s \\ I_s \end{bmatrix} = \begin{bmatrix} [U] & [Z_{se}] \\ & [U] \end{bmatrix} \times \begin{bmatrix} V_r \\ -I_r \end{bmatrix} \tag{7.86}$$

where $[Z_{se}]$ = Diag (series impedance of each phase) and [U] is the identity matrix.

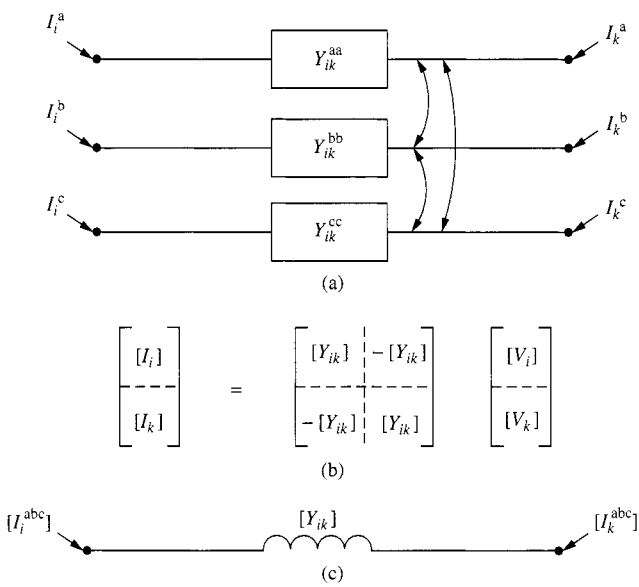

Figure 7.25 Representation of a series element: (a) coupled admittances; (b) admittance matrix; (c) compound admittance

7.10 Distribution System Modelling

The harmonic impedances seen from primary transmission system buses are greatly affected by the degree of representation of the distribution system and the consumer loads fed radially from each busbar. Moreover, the distribution system should also be modelled in the three-phase frame to take into account unbalanced loading, transformers of different connections and earth residual currents.

A typical simplified *dominant* configuration of a distribution feeder is shown in Figure 7.26. Generally, the bulk of the load fed from distribution feeders is located behind two transformers downstream. Thus, to calculate the harmonic impedances seen from the high-voltage primary transmission side it may be sufficient to use a discrete model of the composite effect of many loads and distribution system lines and transformers at the high voltage side of the main distribution transformers; typically the 110 kV in a system using 400 kV and 220 kV transmission.

The following guidelines are recommended for the derivation of distribution feeder equivalents:

- Distribution lines and cables (e.g. 69–33 kV) should be represented by an equivalent-π model. For short lines, the total capacitance at each voltage level should be estimated and connected at that busbar. Due to their relatively low X/R ratio, the resistance of lines and cables plays an important part in damping resonant conditions and should always be included in the equivalent circuit.
- Transformers between distribution voltage levels should be represented by an equivalent element.
- As the active power absorbed by rotating machines does not correspond to a damping value, the active and reactive power demand at the fundamental frequency may not be used in a straightforward manner. Alternative models for load representation should be used according to their composition and characteristics. Groups of small motors may actually provide some damping for the harmonic content depending on the X/R ratio of their blocked rotor circuit.
- Power factor correction (PFC) capacitance should be estimated as accurately as possible and allocated at the corresponding voltage level.
- Other elements, such as transmission line inductors, filters and generators, should be represented according to their actual configuration and composition.

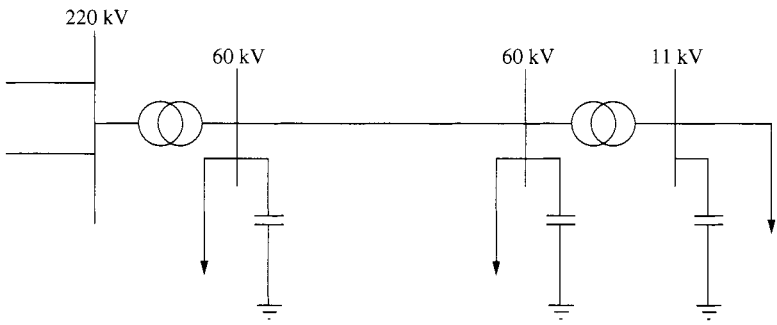

Figure 7.26 Typical distribution feeder

- The representation should be more detailed nearer the points of interest. Simpler equivalents for the transmission and distribution systems should be used only for remote points.
- All elements should be uncoupled three-phase branches, including unbalanced phase parameters.

7.11 Load Models

There are no *generally acceptable* load equivalents for harmonic analysis [25]. In each case the derivation of equivalent conductance and susceptance harmonic bandwidths from specified P (active) and Q (reactive) power flows will need extra information on the actual composition of the load. Power distribution companies will have a reasonable idea of the proportion of each type in their system depending on the time of day and should provide such information.

The aggregate nature of the load makes it difficult to establish models based purely on theoretical analysis. Attempts to deduce models from measurements have been made [26] but lack general applicability. Utilities should be encouraged to develop databases of their electrical *regions,* with as much information as possible to provide accurate equivalent harmonic impedances for future studies.

Consumers' loads constitute not only the main element of the damping component but may affect the resonance conditions, particularly at higher frequencies. Some early measurements [27] showed that maximum plant conditions can result in reduced impedances at lower frequencies and increased impedances at higher frequencies. Simulation studies [28] have also demonstrated that the addition of detailed load representation can result in either an increase or decrease in harmonic flow.

The energy utilisation systems are themselves growing contributors to the harmonic problem as a result of the increased content of nonlinear appliances as explained in Chapter 3.

There are basically three types of loads: passive, motive and power electronic.

(1) Predominantly passive loads (typically domestic) can be represented approximately by a series R, X impedance, i.e.

$$Z_r(\omega) = R_r\sqrt{h} + jX_r h \tag{7.87}$$

where R_r is load resistance at the fundamental frequency, X_r is load reactance at the fundamental frequency and h is harmonic order (ω/ω_1).
The weighting coefficient $\sqrt{h}$, used above for frequency dependence of the resistive component, is different in different models; for instance, reference [25] uses a factor of $0.6\sqrt{h}$ instead. The equivalent inductance represents the relatively small motor content when known. In studies concerning mainly the transmission network the loads are usually equivalent parts of the distribution network, specified by the consumption of active and reactive power. Normally a parallel model is used, i.e.

$$Y_L(\omega) = 1/R_p + j1/(X_p h) \tag{7.88}$$

where R_p is Load resistance at the fundamental frequency, X_p is load reactance at the fundamental frequency and h is harmonic order (ω/ω_1).

$$X_p = \frac{V^2}{Q} \qquad R = \frac{V^2}{P} \tag{7.89}$$

There are many variations of this parallel form of load representation. For example, the parallel load model suggested by reference [25] is a parallel connection of inductive reactance and resistance whose values are

$$X = j\frac{V^2}{(0.1h + 0.9)Q} \qquad R = \frac{V^2}{(0.1h + 0.9)P} \tag{7.90}$$

where P and Q are fundamental frequency active and reactive powers.

(2) Various models of predominantly motive loads have been suggested using resistive-inductive equivalents, their differences being often due to the boundary of system

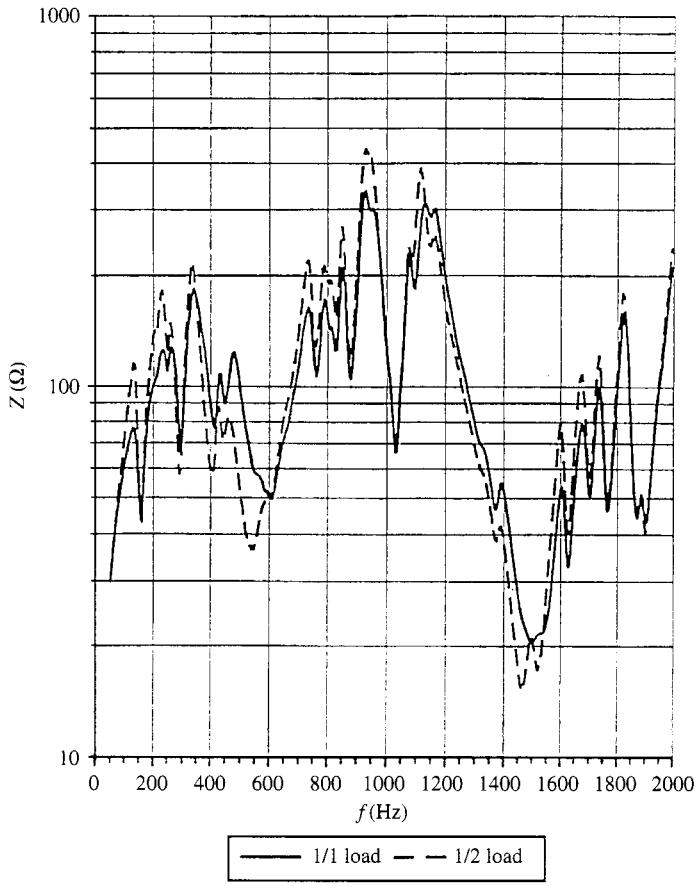

Figure 7.27 Load effect on the magnitude of the network harmonic impedances.(Reproduced from [29] by permission of CIGRE)

representation. A detailed analysis of the induction motor response to harmonic frequencies, leading to a relatively simple model, is described later in this section.

(3) Modelling the power electronic loads is a more difficult problem because, besides being harmonic sources, these loads do not present a constant R, L, C configuration and their nonlinear characteristics cannot fit within the linear harmonic equivalent model. In the absence of detailed information, the power electronic loads are often left open-circuited when calculating harmonic impedances. However, their effective harmonic impedances need to be considered when the power ratings are relatively high, such as arc furnaces, aluminium smelters, etc.

When studying the transmission network it is strongly recommended to model at least part of the next lower voltage level and place the load equivalent there. To illustrate the importance of the loading level on the harmonic impedances, Figures 7.27 and 7.28 show the effect of halving the load level on the magnitude and phase of the individual harmonics at a converter bus connected to a 400 kV system [29].

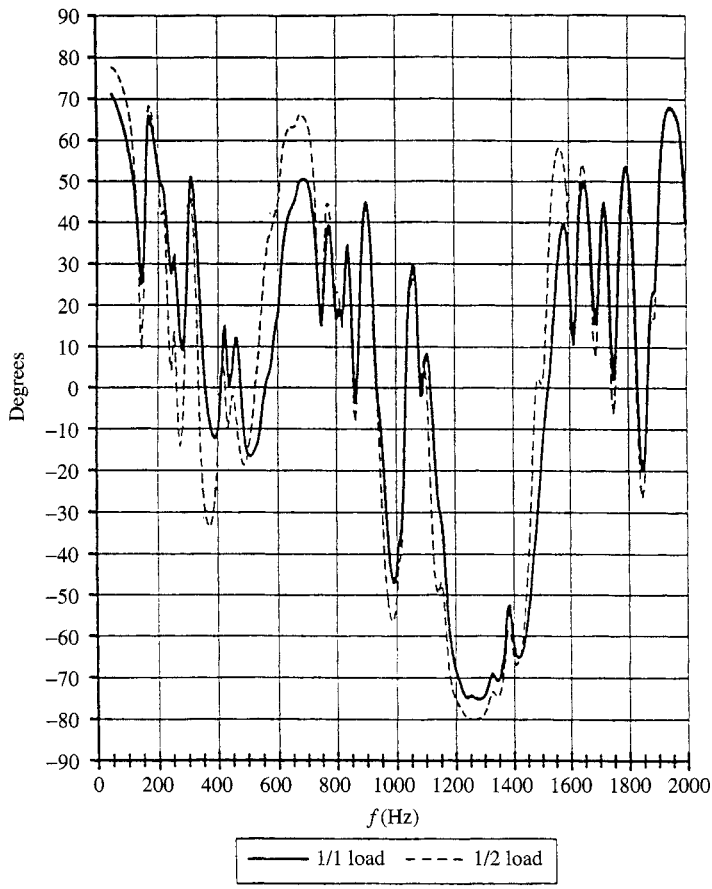

Figure 7.28 Load effect on the phase angle of the network harmonic impedances. (Reproduced from [29] by permission of CIGRE)

7.11.1 Induction Motor Model

The circuit shown in Figure 7.29 is an approximate single-phase representation of the induction motor, with the magnetising impedance ignored.

The motor impedance at any frequency can be expressed as:

$$Z_{\mathrm{m}}(\omega) = R_{\mathrm{mh}} + jX_{\mathrm{mh}} \tag{7.91}$$

At the fundamental frequency ($h = 1$)

$$X_{\mathrm{m1}} = X_1 + X_2 = X_{\mathrm{B}} \tag{7.92}$$

$$R_{\mathrm{m1}} = R_1 + \frac{R_2}{S} = R_{\mathrm{B}}\left(a + \frac{b}{S}\right) \tag{7.93}$$

where R_{B} is the total motor resistance with the rotor locked, R_1 is the stator resistance related to R_{B} by coefficient a (which is typically 0.45), R_2 is the rotor resistance related to R_{B} by coefficient b (which is typically 0.55), and X_{B} is the total motor reactance with the rotor locked.

$$S - \text{Slip} = \frac{\omega_{\mathrm{s}} - \omega_{\mathrm{r}}}{\omega_{\mathrm{s}}}$$

At harmonic frequencies

$$X_{\mathrm{mh}} = h \cdot X_{\mathrm{B}} \tag{7.94}$$

$$R_{\mathrm{mh}} = R_{\mathrm{B}}\left(a.\mathrm{k}_a + \frac{b}{S_{\mathrm{h}}}.k_b\right) \tag{7.95}$$

where k_a, k_b are correction factors to take into account skin effect in the stator and rotor, respectively, and S_{h} is apparent slip at the superimposed frequency, i.e.

$$S_{\mathrm{h}} = \frac{\pm h\omega_{\mathrm{s}} - \omega_{\mathrm{r}}}{\pm h\omega_{\mathrm{s}}} \tag{7.96}$$

$$S_{\mathrm{h}} \approx 1 - \frac{\omega_{\mathrm{r}}}{h\omega_{\mathrm{s}}} \quad \text{for the positive-sequence harmonics}$$

$$S_{\mathrm{h}} \approx 1 + \frac{\omega_{\mathrm{r}}}{h\omega_{\mathrm{s}}} \quad \text{for the negative-sequence harmonics}$$

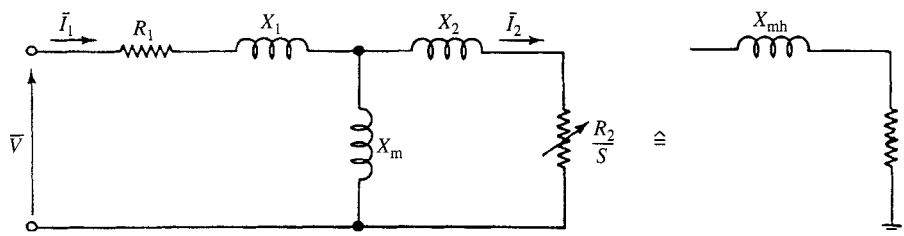

Figure 7.29 Approximate representation of the induction motor

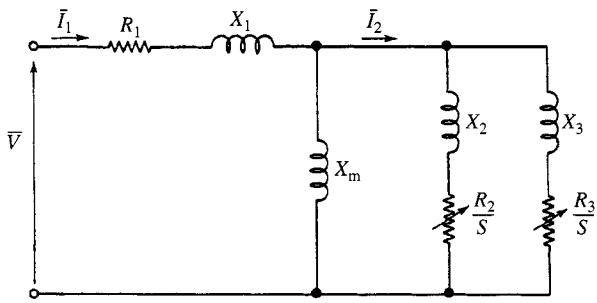

Figure 7.30 Accurate induction motor model

Assuming an exponential variation of the resistances with frequency, i.e.

$$k_a = h^{\alpha}$$

$$k_b = (\pm h - 1)^{\alpha}$$

the motor equivalent resistance for $\alpha = 0.5$ becomes

$$R_{mh} = R_B[a\sqrt{h} + (\pm h.b\sqrt{\pm h - 1})/(\pm h - 1)] \tag{7.97}$$

An accurate model of a double cage induction motor is shown in Figure 7.30.

7.11.2 Norton Equivalents of Residential Loads

In practice there is always a mix of the three types of load and no general guidelines can be given for their representation without detailed knowledge of their composition. However, the latter are reasonably predictable in the case of radial distribution systems feeding domestic customers. In these cases, and with judicious estimation of the load mix, it is possible to derive accurate equivalents for the composite residential load.

The Pspice program is used in reference [30] to derive equivalent components for specified combinations of linear and nonlinear appliances as well as the low-voltage distribution network of a residential feeder. The nonlinear appliances include personal computers, compact fluorescent lamps, television sets and fluorescent lighting. It is a bottom-up approach, whereby the instantaneous voltages and currents of the network are calculated and then the Fourier transform of the waveshapes obtained. The linear load is represented as a single branch with a lumped circuit derived at the point of common coupling (PCC) [31].

The different load combinations used in the test system were decided based on extensive household interviews in the area. The third, fifth and seventh harmonic currents on the LV side of the distribution transformer were also monitored over a period of several days for the purpose of model verifications. The simulation results substantially agreed with the recorded values.

While requiring considerable effort, this approach can be used to derive harmonic equivalent circuits at PCCs of residential feeders to be used in further system

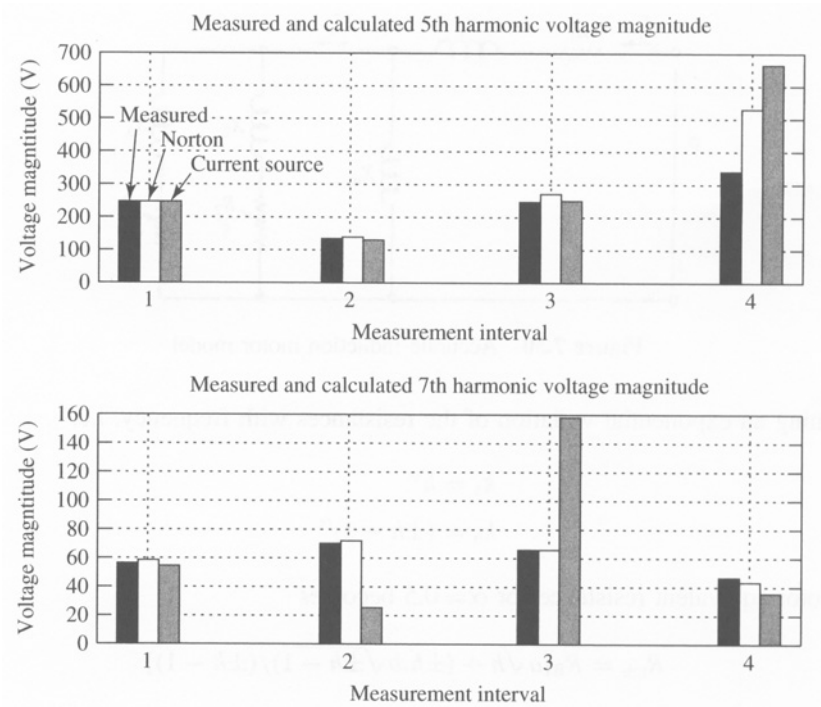

Figure 7.31 Measured and calculated harmonic voltage magnitude

development. It is envisaged, however, that the application of this method to industrial feeders is not straightforward considering the greater variety of their loads and operating cycles.

7.11.3 Empirical Models Based on Measurements

An alternative approach to explicit load representation is the use of empirical models derived from measurements.

In particular, information obtained from harmonic current and voltage measurements with different operating conditions, for example by switching a shunt capacitor (as described in Section 7.3.1), can be used to derive approximate Norton harmonic equivalents of the load or group of loads connected at a distribution bus. By way of example, Figure 7.31 shows measured and calculated harmonic voltages at four 10-minute time intervals for an 11 kV distribution bus fed from the 220 kV transmission system via a 40 MVA transformer [32]. Clearly the Norton approach gives a better estimation of the harmonic voltages than the constant current source.

7.12 Computer Implementation [33]

The evolution of computer technology has removed many of the limitations that affected implementation decisions in the past.

Earlier implementations were restricted by the use of mainframe computers, and limitations in graphical support, memory and storage space.

The main factor affecting recent implementations has been the acceptability of the personal computer (PC) as the main computing platform in terms of capability and price. The PC platform has been enhanced by the use of several graphical operating systems and particularly Microsoft Windows™. Other important developments have been the availability of ample computer bandwidths, reduced cost of memory modules, making memory limitation secondary, cheaper storage modules with much larger capacity, and great improvement in software support and development support tools.

To cope with the larger size and complexity of computer programs, new facilities have become available to make the software more modular and easier to maintain. Three important examples are multitasking operating systems, graphical user interfaces (GUIs), and object-oriented design methodology.

In line with the steps described in the previous sections of the chapter, the computer implementation involves the following stages:

- Computation of the admittance matrices of individual components at the specified harmonic frequencies.
- Formation of the system admittance matrices at individual frequencies according to the network topology.
- Calculation of the system harmonic voltages at all the system nodes given the harmonic current injections at the nodes containing nonlinear plant components.

7.12.1 Harmonic Penetration Overview

A modern harmonic penetration program includes a GUI, the simulation algorithm engine and a database handling data structure.

The GUI is used for data entry (component parameters and network topology), and for the presentation of the simulation results.

The simulation algorithm engine performs the calculations required and has traditionally been written in the FORTRAN language, although recently object-oriented languages have also been used. Mixed-language programming makes it possible to use FORTRAN's advantage of built-in complex number manipulation with other languages to benefit from the strengths of each.

Database handling routines are used to store and retrieve the power system data from disk. However, the traditional fixed format, still widely used today, is very rigid and inflexible. The use of a platform-independent text format, such as ASCII, provides far greater flexibility.

7.12.2 An Advanced Program Structure

Lack of memory space has in the past forced simulation packages to be fragmented into several programs. Moreover, lack of computer power has often made it necessary to store intermediate results rather than recalculate them as and when needed.

The structure of a typical software package for harmonic analysis is illustrated in Figure 7.32. The computational effort required to generate the harmonic admittance matrices of transmission lines and cables usually exceeds that of forming the system admittance matrix and solving for the harmonic voltages and currents. Therefore, these matrices are usually computed separately and stored in disk files, which are then read by the main simulation program when forming the system admittance matrices. The modelling of nonlinear loads is also separated from the main program; the calculated current injections are then stored in disk files and read by the main program when performing the harmonic penetration analysis. The results of the harmonic penetration study are also output to disk files to be imported into plotting tools for presentation. These can also be used by other tools such as Matlab™ for further analysis or spreadsheets for reporting purposes.

Although the above subdivisions have enabled complex analysis to be performed successfully despite the limitations presented by earlier computers, their main drawback is the use of many intermediary files, the maintenance of which becomes laborious when the simulated system is large, as all these files must be updated before the succeeding program is activated. Moreover, the conversion of complex or floating numbers into the text format typically used in these files introduces truncation or round-off errors. These errors may distort the final results, especially at high harmonic frequencies when the distortion levels are generally low, particularly when the analysis process involves many such conversions. The use of unformatted data has the advantages of reduced file size, and faster reading and writing to disk operations without introducing truncation errors; however, the data in the file cannot be readily inspected.

Typically, a graphical data entry or editor is added to the package to help the user to construct the simulation cases. These editors are usually separate applications that are able to generate the necessary data files required in the simulation. The simulation results are imported into plotting applications such as Matlab™ or Microsoft Excel™ for further analysis or reporting purposes.

Several advances in computer technology have made it possible to integrate all the above processes into a single framework without the need to combine them all into a single huge executable binary. The most important developments are abundance of cheap memory (which includes virtual memory and dynamic memory allocation

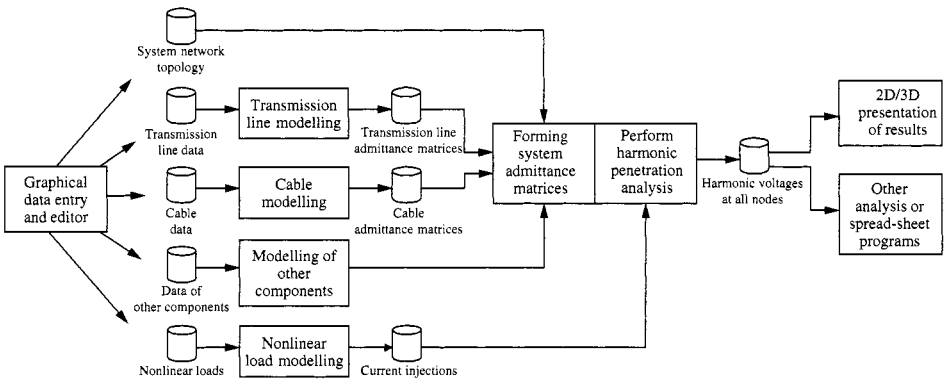

Figure 7.32 Structure of harmonic analysis software

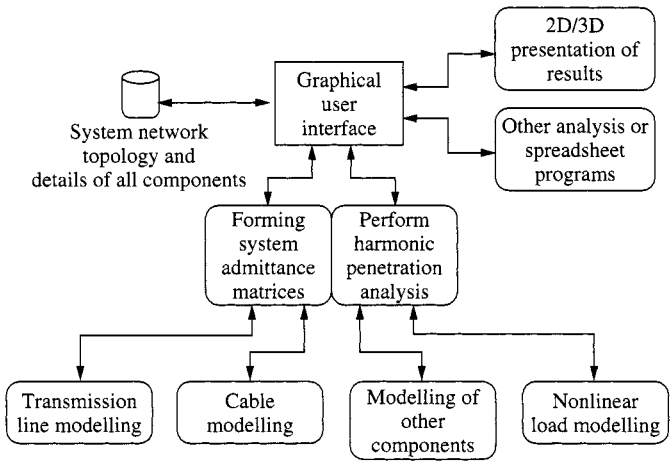

Figure 7.33 Functional overview

technologies), dynamic linked libraries, object-oriented development tools and mixed-language programming.

Making use of these new technologies, Figure 7.33 depicts how a harmonic penetration simulation program is put together. The mathematical modelling of the power system components, including nonlinear loads, and the harmonic penetration are programmed as relocatable dynamic linked libraries and these are made accessible to the GUI. Through this GUI, users can construct the power system simulation network by joining different power system components together and specifying the component parameter settings. The constructed simulation network consists of lists of power system components and their settings; these are passed to the harmonic penetration library to carry out the tasks required by the simulation study.

7.12.3 Data Structure

The essence of the object-oriented methodology is a family of classes that make up the application. Each of the classes has its own unique properties or settings and includes procedures to alter the settings. At execution, objects of the classes are created when they are needed to perform certain tasks and they are usually deleted upon completion of these tasks.

The data used in the harmonic penetration study includes the power system components and the topology by which they are connected to form a system. Therefore, based on the object-oriented methodology, a simulation case can be regarded as a drawing page or canvas object, which acts as a container for all the power system components objects making up the system. The various classes of objects making up an object-oriented version of harmonic analysis are summarised in Figure 7.34.

The two main classes are the Power System Canvas and the Power System Component class, both inherited from the Generic Graphical Component, which provides the interfaces to the low-level graphical functions of the GUI operating system (which is Microsoft Windows™ in this implementation).